SIDT1 plays a key role in type I IFN responses to nucleic acids in plasmacytoid dendritic cells and mediates the pathogenesis of an imiquimod-induced psoriasis model

María Morell,[a] Nieves Varela,[a] Casimiro Castillejo-López,[a,1] Céline Coppard,[a] María José Luque,[a] Ying-Yu Wu,[b] Natividad Martín-Morales,[c,d] Francisco Pérez-Cózar,[a] Gonzalo Gómez-Hernández,[a] Ramesh Kumar,[b] Francisco O'Valle,[c,e] Marta E. Alarcón-Riquelme,[a,f] and Concepción Marañón[a]*

[a]GENYO, Centre for Genomics and Oncological Research. Pfizer, University of Granada, Andalusian Regional Government, Avda Ilustración 114, PTS Granada 18016, Spain
[b]Arthritis and Clinical Immunology Program, Oklahoma Medical Research Foundation, Oklahoma City, Oklahoma, USA
[c]Department of Pathology, School of Medicine, University of Granada, Spain
[d]Department of Oral Surgery, School of Dentistry, University of Granada, Spain
[e]Ibs.GRANADA and IBIMER Institutes, Spain
[f]Institute for Environmental Medicine, Karolinska Institutet, Stockholm, Sweden

EBioMedicine 2022;76: 103808
Published online xxx
https://doi.org/10.1016/j.ebiom.2021.103808

Summary

Background Type I IFN (IFN-I) is a family of cytokines involved in the pathogenesis of autoimmune and autoinflammatory diseases such as psoriasis. SIDT1 is an ER-resident protein expressed in the lymphoid lineage, and involved in anti-viral IFN-I responses *in vivo*, through an unclear mechanism. Herein we have dissected the role of SIDT1 in the natural IFN-producing cells, the plasmacytoid dendritic cells (pDC).

Methods The function of SIDT1 in pDC was determined by silencing its expression in human primary pDC and GEN2.2 cell line. SIDT1 role *in vivo* was assessed using the imiquimod-induced psoriasis model in the SIDT1-deficient mice (*sidt1*$^{-/-}$).

Findings Silencing of SIDT1 in GEN2.2 led to a blockade of the IFN-I response after stimulation of TLR7 and TLR9, without affecting the pro-inflammatory responses or upregulation of maturation markers. We found that SIDT1 migrates from the ER to the endosomal and lysosomal compartments together with TLR9 after CpG stimulation, participating in the access of the TLR9-CpG complex to lysosome-related vesicles, and therefore mediating the activation of TBK1 and the nuclear migration of IRF7, but not of NF-κB. *sidt1*$^{-/-}$ mice showed a significant decrease in severity parameters of the imiquimod-induced acute psoriasis-like model, associated with a decrease in the production of IFN-I and IFN-dependent chemokines.

Interpretation Our findings indicate that SIDT1 is at the cross-road between the IFN-I and the proinflammatory pathways and constitutes a promising drug target for psoriasis and other diseases mediated by IFN-I responses.

Funding This work was supported by the Consejería de Salud y Familias de la Junta de Andalucía (PIER_S1149 and C2_S0050) and Instituto de Salud Carlos III (PI18/00082 and PI21/01151), partly supported by European FEDER funds, and prior funding to MEAR from the Alliance for Lupus Research and the Swedish Research Council.

Keywords: SIDT1; pDC; IFN-I; Proinflammatory cytokines; TLR7; TLR9; IRF7; Psoriasis

Introduction

Psoriasis is a paradigm among the interferon-dependent autoimmune diseases, characterized by the detection of an "IFN signature" in blood and tissues[1]. Indeed nucleic acid-induced IFN-I production plays a prominent role in the initial immunopathogenic steps of

*Corresponding author.
E-mail address: concepcion.maranon@genyo.es (C. Marañón).

[1] Present address: Department of Immunology, Genetics and Pathology, Uppsala University, Sweden

Research in context

Evidence before this study

The functionality of the multi-span transmembrane protein SIDT1 in mammals has remained elusive for a long time. Only recently, few papers have reported a role of SIDT1 in the uptake and intracellular transport of dietary cholesterol, as well as in the induction of antiviral IFN-I responses *in vivo*. SIDT1 is mostly expressed in lymphoid cells, suggesting a specialized function in these cells.

Added value of this study

This work is centered in the plasmacytoid dendritic cells (pDC), which are the master organizers of the antiviral IFN-I responses. They are also key in the initiation of the immunopathological events of IFN-mediated diseases, such as psoriasis. We show that SIDT1 is in the crossroad between IFN-I and proinflammatory responses and SIDT1 silencing or knock-out impairs IFR7 activation and protects mice using an induced psoriasis model.

Implications of all available evidence

A tight control of the balance between IFN-I and proinflammatory responses in pDC is key for a protective antiviral immune response and to avoid the appearance of autoimmune and autoinflammatory diseases. Thus, SIDT1 is a promising target for the design of immune modulators for these diseases.

psoriasis and other autoimmune disorders.[2,3] In the search for new therapies for IFN-mediated diseases, IFNα/β-blocking strategies are appealing.[4] Current clinal trials are mainly focused on anti-IFN or -IFNα/β receptor monoclonal antibodies, but other molecules of the pathway have also being tested, as reviewed in.[5] pDC are professional IFN-producing cells capable of secreting it in large amounts.[6] They secrete actively proinflammatory cytokines, chemokines and type I and III IFN following recognition of pathogen and danger-related nucleic acids through the endosomal Toll-like receptors TLR7 (sensing single-stranded RNA) and TLR9 (sensing unmethylated CpG-containing double-stranded DNA), as well as an array of cytosolic sensors.[5] A tight balance between proinflammatory cytokines and IFN-I is crucial and thus, inappropriate pDC endosomal TLR responses are considered key in the physiopathology of IFN-mediated diseases,[7–10] and are also involved in non-protective anti-viral responses.[11,12]

TLR7 and TLR9 reside in the endoplasmic reticulum (ER) in resting pDC and translocate to endosomal vesicles to encounter their ligands.[13,14] After ligation, the receptors are cleaved, allowing for recruitment of the adaptor protein MyD88 followed by the transcription of NF-κB-dependent proinflammatory cytokines and IRF7-dependent IFN-I responses. Since different signals arise from different endocytic compartments,[15] it is considered that TLR9-containing vesicles bifurcate from NF-κB-endosomes to IRF7-endolysosomes.[16,17] Accordingly, several proteins involved in the lysosomal pathway have been involved in IFN-I production by pDC,[17,18] and chloroquine inhibition of endosomal acidification interferes with IFNα responses to TLR7 and TLR ligands in pDC.[19,20] While much of the characterization of this traffic is characterized using TLR9, it is likely that TLR7 signaling and trafficking uses the same pathways.[21]

SIDT1 is a multispan transmembrane protein belonging to the SID1 transmembrane family, with certain sequence homology to *C. elegans* ChUP-1, a cholesterol-binding protein located in intracellular vesicles,[22,23] and involved in the immune responses of the nematode.[24] SIDT2 is ubiquitously expressed and has a role in the induction of proinflammatory and IFN-I antiviral responses mediated by cytosolic dsRNA sensors.[25] However, SIDT1 is mainly expressed in the lymphoid lineage and seems to have a role in the anti-viral IFN-I responses *in vivo* thought an unknown mechanism.[26]

Herein we explore the role of SIDT1 in the main IFN-producing cells, the pDC. We demonstrate that SIDT1 is involved specifically in the IFN-I but not in the pro-infammatory responses in human and mouse pDC models, being an essential point of bifurcation in the TLR7/9 signaling pathway between the IFR7 and the NF-κB cascades. SIDT1 is required for the access of the TLR/ligand complexes to the endolysosomal vesicles, and it promotes the activation of the TBK1/IRF7 axis. Additionally, we evaluate the role of SIDT1 *in vivo* in an autoimmune disease model dependent of the IFN-I response and based on TLR7 stimulation, the imiquimod-induced psoriasiform skin inflammation model.[27] *sidt1*$^{-/-}$ animals show a decrease in severity, associated with an important reduction of the IFN-I level in serum and IFN-dependent chemokines in the skin lesions.

Methods

Mice

sidt1$^{-/-}$ mice (MGI Cat# 5292890, RRID: MGI:5292890) were generated at the University of California Davis and the Children's Hospital Oakland research Institute, as part of the Knockout Mouse Project,[28] using ES cells and Velocigene vector and a reporter-tagged deletion allele strategy in a C57BL/6 background and has been described before.[26,29] SIDT1 transcripts were undetectable in the spleen of *sidt1*$^{-/-}$ mice by qRT-PCR ([26] and laboratory data). The mouse strain was maintained at heterozygosis under pathogen-free conditions at the University of Granada (Centro de Investigaciones Biomédicas) animal facilities. Littermate WT C57Bl/6 animals (IMSR Cat# JAX:000664, RRID:IMSR_JAX:000664) were used as controls in all the experiments.

Cell lines and stimulation

The cell line HEK-293 (CLS Cat# 300192/p777_HEK293, RRID:CVCL_0045), was obtained from ATCC. GEN2.2 cell line (RRID:CVCL_5G44)[30] was obtained from the CNCM of Pasteur Institute. Both cell lines were validated by the corresponding repositories and used before passage 10. Additionally, they were validated using short tandem repeat analysis (STR). The cell lines were regularly tested for mycoplasm contamination using the Venor®GeM qEP Mycoplasma Detection Kit for qPCR (Minerva Biolabs, Cat#11-9250), and all the experiments were performed using mycoplasma-free cells. All cell lines were cultured at 37 °C and 7% CO2 in a humidified incubator.

GEN2.2 cells were cultured at a density of 7.5×10^5 cells/ml in RPMI 1640 medium containing Glutamax (Life Technologies) supplemented with 10% fetal bovine serum (FBS, Biowest), 1% nonessential amino acids, 1 mM sodium pyruvate 100 U/ml penicillin and 100 mg/ml streptomycin (Life Technologies) and were stimulated for the indicated time in duplicates with 1 μM ODN2006 (Life Technologies) 1 μM ODN2216 (Sigma-Aldrich), 3 μg/ml imiquimod or resiquimod (both from Invivogen) except for titration experiments. For the stimulation of cytosolic sensors, cells were stimulated 20 μg/ml PolyI:C (Invivogen) or 1 μM ODN2006 plus Lipofectamine 2000 (Life Technologies) as in.[31] HEK293 cells were cultured in Dulbecco's modified Eagle's medium (DMEM) supplemented with 10% FBS, 1% nonessential aminoacids. HEK-Blue IFNα/β (RRID:CVCL_KT26) and B16-blue IFNα/β (RRID:CVCL_X605) indicator cells were obtained from Invivogen and cultured in the presence of 100 μg/ml zeocin (Invivogen) and 10 μg/ml blasticidin (Fisher Scientific).

Cell transfection and viral transduction

Stable HEK293T cell transfectants were obtained by lipofection with 2 μg of each DNA vector (TLR9-YFP and SIDT1-CFP in pcDNA) into 200 μl of jetPRIME buffer containing 4 μl of Jet Prime (Polyplus Transfection, VWR, Cat#114-15) following the manufacturer instructions. 24 h after lipofection the medium was replaced and 1 mg/ml G418 was added. After antibiotic selection double-positive (TLR9-YFP and SIDT1-CFP) or single positive cells were purified by flow cytometry cell sorting using a FACS Aria II device (BD Biosciences).

For SIDT1 silencing, GEN2.2 cells were transduced with lentiviral particles derived from pLenti-H1-RSV (GFP-Bsd) vectors (AMSBIO) coding for GFP protein and containing three different SIDT1-specific shRNA (Fig. S1a) at a moi = 1 each. After 6 h the lentiviral particles were washed, and transduced cells were selected using 10 μg/ml blasticidine after 48 h of culture. As a control, GEN2.2 cells were transduced with a universal null shRNA control sequence in the same conditions. shSIDT1 and shCTL transduced cells were stored frozen in liquid nitrogen after selection and validated by STR. Cells were used with a maximum of 10 passages to ensure stability of the phenotype.

Primary cell isolation and stimulation

For human pDC purification peripheral blood mononuclear cells (PBMC) were isolated from blood units of healthy donors tested for HIV, HBV, and HCV (Centro Regional de Transfusión Sanguínea, Granada) by density-gradient centrifugation using LSM 1077 Lymphocyte Separation Medium. A total of 7 donors were recruited for this study. All donors signed an informed consent form according to the ethical protocols of the Andalusian Biobank. pDC were purified by positive selection using the BDCA-4/neuropilin-1 microbead kit in an AutoMACS device (both from Miltenyi Biotec) following the recommendations of the provider. The purity of the pDC preparation ranked between 90–95% as evaluated by flow cytometry using BDCA-2 (Miltenyi Biotec Cat# 130-113-190, RRID:AB_2726015) and CD123 (BioLegend Cat# 306015, RRID:AB_2124258) specific antibodies (Fig. S2a).

Purified pDC were resuspended at a density of 10^6 cells/ml in RPMI supplemented with 5% autologous plasma, and dispensed in round-bottom 96-well plates in duplicates. The cells were stimulated with 1 μM ODN2006 (Life Technologies) or 1.25 μg/ml resiquimod (Invivogen) for 24 h at 37 °C. For SIDT1 silencing pDCs were transduced with shSIDT1 or shCTL lentiviral particles at a moi = 2 and simultaneously stimulated with 1 μM ODN2006 (Life Technologies) for 18 h at 37 °C. Afterwards cell pellets and supernatants were harvested and tested for GFP expression by flow cytometry, for SIDT1 mRNA expression by digital RT-PCR (dPCR), or IFN-I and TNFα secretion as described below.

Spleens from 12 to 16 weeks old WT and *sidt1*$^{-/-}$ male animals were obtained in sterile conditions and homogenized. The erythrocytes were lysed using ACK (Ammonium-Chloride-Potassium) lysing buffer. Bone marrow-derived pDC (BM-pDC) were differentiated from bone marrow cells from 12 to 16 weeks-old female mice in the presence of 200 ng/ml FLT3L for 8 days as in.[32] Cells were seeded at 4×10^6 cells/ml in 12-well plates in the presence or absence of 1 μM ODN2216 (Life Technologies), 3 μg/ml resiquimod or 5 μg/ml imiquimod (Invivogen). Supernatants were collected at 48 h and assayed for TNFα and IFN-I as described below.

Imiquimod-induced acute psoriasis-like mouse model

12–16 weeks-old WT C57BL/6 and *sidt1*$^{-/-}$ male mice were shaved on the back skin and randomized in the placebo (vaseline) and treated (imiquimod) groups. The imiquimod-treated animals received a topical application of 62.5 mg of 5% imiquimod cream (Aldara, Meda AB), or the equivalent amount of vaseline on the back

and in the right ear, every second day over 6 consecutive days. At day 6, inflammation severity of the back skin was scored (scale 0–12), following the clinical Psoriasis Area and Severity Index (PASI) with small modifications;[33] since in the mouse model the extent of the affected area of the skin cannot be taken into account in the total score, the combined score was calculated including three parameters ranking from 0 to 4: erythema, scales, and thickening. The score was obtained blindly by two independent researchers.

Spleen, treated and untreated skin were recovered for further tests. A fraction of the skin samples was stored at -80 °C for cytokine detection, and the remaining skin material was fixed for histological analysis.

Cytokine and chemokine quantification

Supernatants from stimulated cells were harvested at the indicated time points. Sandwich ELISA kits were used to detect mouse TNFα (Thermo Fisher Scientific Cat# 88-7324-86, RRID:AB_2575079) and human IL-6 (Thermo Fisher Scientific Cat# 88-7066-88, RRID: AB_2574995), IL-8 (Thermo Fisher Scientific Cat# 88-8086-86, RRID:AB_2575174), TNFα (Thermo Fisher Scientific Cat# 88-7346-86, RRID:AB_2575096), CCL3 (Thermo Fisher Scientific Cat# 88-7035-88, RRID: AB_2574962), IFNα (Thermo Fisher Scientific Cat# BMS216TEN, RRID:AB_2575463), IL-29 (IFNλ1) (Thermo Fisher Scientific Cat# 88-7296-88, RRID: AB_2575064), following standard protocols. The absorbance at 450 and 570 nm was measured in an Infinite M200Pro plate reader (Tecan). IFNα/β activity was quantified in U/ml using the indicator cell lines HEK-Blue IFNα/β (RRID:CVCL_KT26) and B16-Blue^{TM} ISG-KO-STING (RRID:CVCL_X603) for human and mouse respectively. The QuantiBlue colorimetric assay (Invivogen) was used for human IFN-I, while BM Chemiluminiscence ELISA substrate AP kit (Roche) was used for mouse IFN-I to reach a higher sensitivity. Recombinant human IFNα2a and recombinant mouse IFNα (Miltenyi Biotec) were used as standards.

Frozen mouse skin samples were harvested and homogenized in Tissue Protein Extraction Reagent (T-PER, Thermo Scientific) supplemented with Protease Inhibitor Cocktail (Thermo Scientific) using steal beads in a Tissue Lyser LT (QIAGEN). After centrifugation, supernatants were collected and the protein concentration in the lysate was determined using the BCA kit (Thermo Fisher). Finally, a lysate containing 3 µg/ml of total proteins was used for cytokine detection as in.[34] Cytokine levels were quantified using the Cytokine & Chemokine 36-plex Mouse ProcartaPlex Panel 1A kit (Thermo Fisher, EPX360-36092-901) in a Luminex-200 reader (Luminex Corp.), following the protocol recommended by the vendor.

Histology

Back skin samples were collected at day 6 as described before, fixed in 10% buffered formalin for 48 h and paraffin-embedded. After deparaffination, sections were stained with hematoxylin/eosin (H&E), and movat pentachrome[35] for morphological studies. The histopathological evaluation was done in a blinded fashion by two operators on 4-micrometer sections under a light microscopy Olympus BX43 (Olympus Optical Company, Ltd., Tokyo, Japan).

Morphological psoriasis-like acute model changes in the section of the back skin (hyperkeratosis, parakeratosis, confluent parakeratosis, Munro microabscesses, spongiform pustules of Kogoj, hypergranulosis, acanthosis, spongiosis, pseudopapillomatosis, dilated vessels, RBC extravasation, and perivascular lymphocytes) were semiquantitatively evaluated using H&E and movat pentachrome-stained slides, as dichotomous variables (presence or absence in each mouse). The number of mitoses in epithelium was established by ten high power field (HPF). Area (in square millimeters) and percentage of the epithelium; suprapapillary and rete ridge thickness of the epithelium were measured (in millimeters) on light microscopy images (original magnification 2x) using the DP70Controller program (Olympus) and the open source image processing program ImageJ V. 1.48 (https://imagej.nih.gov/ij/). A millimeter scale in the eyepiece of a BH2 microscope (Olympus) with 40x objective was used to count dermal inflammatory cells, per mm^2. Keratin deposit areas were measured by averaging 3-4 fields of each skin section per animal using ImageJ.

Flow cytometry

For ODN2006 endocytosis studies, shSIDT1 GEN2.2 cells and their controls were incubated with 5 nM ODN2006-Cy5 (Life Technologies) in triplicates, and the fluorescence at Cy5 channel was measured at different time points in a FACS Verse flow cytometer. The geometric mean fluorescence intensity was quantified using FlowJo X.0.7 software. For antibody labeling, PBMC, pDC, BM-pDC or GEN2.2 cell suspensions were blocked for 15 min in FACS buffer (0.5 % BSA, 2 mM EDTA in PBS) and labeled with fluorescent antibodies for 15 min at room temperature in the dark. Afterwards, cells were washed and resuspended in the same buffer. For cell lines and purified pDC a minimum of 10,000 live cells were acquired, while at least 100,000 live cells were acquired in the case of PBMC. Data were acquired on a FACS Verse flow cytometer (BD) and analyzed using FlowJo X.0.7 software.

The antibodies used were human αBDCA-2-APC (Miltenyi Biotec Cat# 130-113-190, RRID:AB_2726015), αCD123-PerCP-Cy5.5 (BioLegend Cat# 306015, RRID: AB_2124258), αCD80-PE (BioLegend Cat# 305207, RRID:AB_314503), αCD86-PE (BioLegend Cat# 374205, RRID:AB_2721632), αCD40-PerCP-eFluor710, (eBioscience Cat # 46-0409-42 RRID:AB_1834403). For mouse studies the following antibodies were used: αI-

A/I-E-PerCP-Cy5.5 (Thermo Fisher Scientific Cat # A14902 RRID:AB_2534340), αCD86-PE, (Thermo Fisher Scientific Cat# MA1-10296, RRID: AB_11156810), αSiglecH-PECy7 (Thermo Fisher Scientific Cat# 25-0333-82, RRID:AB_2573342), αCD40-FITC, (Thermo Fisher Scientific Cat# 11-0402-82, RRID:AB_465029).

Image flow cytometry

For transcription factor translocation studies, GEN2.2 cells and mouse BM-pDC were stimulated at a density of 2×10^6 cells/ml with ODN2006, ODN2216, respectively (Life Technologies), and resiquimod for the indicated time points at 37 °C. Afterwards the cells were fixed with 2% paraformaldehyde for 15 min at RT and permeabilized with 1% BSA, 0.02% saponin in PBS for 5 min at RT. After 20 min at RT in blocking buffer (3% goat serum in PBS), the cells were washed for 5 min at 800 x g at RT and stained with αhIRF7-AlexaF647 (Thermo Fisher Scientific Cat# 51-5375-42, RRID: AB_2716969), αh/mNF-kB p65 (Cell Signaling Technology Cat# 8242, RRID:AB_10859369) or αmIRF7-PE (Thermo Fisher Scientific Cat# 12-5829-80, RRID: AB_2572628) antibodies for 1h at RT. A goat αrabbit IgG-Alexa488 (Thermo Fisher Scientific Cat# A32731, RRID:AB_2633280) and a goat αmouse IgG-Alexa555 (Thermo Fisher Scientific Cat# A-21422, RRID: AB_2535844) were used as secondary antibodies. Finally, cells were washed with PBS and nuclei were stained with 1 μM Hoechst 33342 (Thermo Fisher). The samples were washed and resuspended in FACS buffer before acquisition.

At least 10,000 cell images were acquired in an ImagestreamX Mark II imaging flow cytometer (Amnis), using a 60 × magnification and low speed in high resolution. Single color controls for each of the specific markers at the concentrations used above were also acquired and subsequently used for compensation. Compensated files were analyzed using the nuclear localization wizard in the IDEAS 6.2 software (Amnis).

Immunoblotting

After stimulation, 2×10^6 cells were washed with ice-cold PBS, resuspended at 2.5 10^4 cells/μl in A-Lysis Buffer (10 mM HEPES; 10 mM KCL; 0.1 mM EGTA pH 7.9; 1 mM DTT; 1 mM PMSF; protease and phosphatase inhibitor cocktail (Roche)) for 15 min on ice. Afterwards, 1.25% NP-40 was added, and the cells were lysed for 10 s and centrifuged at 13,000 g for 5 min at 4 °C. The supernatant was conserved as the cytosolic fraction. The pellets containing the nuclei were washed in PBS, lysed in 30 μl B-Lysis Buffer (20 mM HEPES, 0.4 M NaCL, 1 mM EGTA; 1 mM EDTA, 1 mM DTT, 0.5 mM PMSF, protease and phosphatase inhibitor cocktail (Roche)) for 15 min on ice in agitation. The supernatant containing nuclear lysate was collected after centrifugation at 13,000 rpm for 5 min at 4 °C. Protein concentration was quantified using the Bradford method (BioRad).

The cellular extracts (30 μg protein) were mixed with 1X NuPAGE LDS Sample Buffer reducing agent (Life Technologies) plus 0.2 M DTT (Sigma-Aldrich), and were denatured by heating at 95 °C for 5 min. Lysates were electrophoresed using 4−15% gradient SDS-PAGE gels (BioRad), transferred to PVDF membranes using a Transblot device (BioRad), and the target proteins were detected with the appropriate antibodies following standard procedures. Images were analyzed using ImageJ software v1.48. The antibodies used were: αhSIDT1 (Santa Cruz Biotechnology,Cat#sc-390015, RRID: AB_2884957), αHDAC1 (Santa Cruz Biotechnology Cat# sc-81598, RRID:AB_2118083), αTBK1 (Cell Signaling Technology Cat# 3013, RRID:AB_2199749), αpTBK1 (Ser172) (Cell Signaling Technology Cat# 5483, RRID:AB_10693472), αactin (Sigma-Aldrich Cat# A2547, RRID:AB_476701). Secondary antibodies were αrIgG-HRP (Santa Cruz Biotechnology Cat# sc-2357, RRID:AB_628497) and αmIgG-HRP (Santa Cruz Biotechnology Cat# sc-2005, RRID:AB_631736).

RNA analysis

Total RNA was isolated from cells using High Pure RNA isolation Kit (Roche Diagnostics Cat# 11828665001) according to the manufacturer's instructions and cDNA was synthesized from 1 μg total RNA using the First-Strand cDNA Synthesis Kit (Roche Diagnostics Cat# 04379012001). The quantity and integrity of the RNA were evaluated using a Nanodrop 2000 device (ThermoScientific) and a 2100 Bioanalyzer (Agilent). The samples with RIN values > 9 were selected. cDNA was obtained using Transcriptor First Strand cDNA Synthesis kit (Roche).

SIDT1 mRNA was quantified by digital RT-PCR (dPCR) using the QuantStudio 3D Digital PCR System (Life Technologies), according to the manufacturer's recommendations. Reactions were performed in a final volume of 18 μL containing Quantstudio 3D Digital Master Mix v2, TaqMan assay-FAM, TaqMan assay-VIC, nuclease-free water and template cDNA. Samples were loaded onto chips using the QuantStudio 3D Digital Chip Loader (Life Technologies) and cycled according to the following parameters: 96 °C for 10 min, followed by 45 cycles at 57 °C for 2 min, and 98 °C for 30 s and a final elongation step at 57 °C for 7 min. The following TaqMan probes (Life Technologies) were used: SIDT1-FAM (Hs00214475_m1) as target gene and TBP-VIC (Hs00427620_m1) as housekeeping. After thermocycling, the QuantStudio™ 3D Digital PCR Instrument (Life Technologies) and the QuantStudio™ 3D AnalysisSuite™ Software (Life Technologies) were used to collect and analyze the end-point fluorescence data of each chip.

For RNA expression array analysis, WT, shCTL and shSIDT1 GEN2.2 cells growing at log phase were stimulated with 1 μM ODN2006 for the indicated time points in triplicates, and total RNA was isolated as before. A total of 300 ng of total RNA was processed using Illumina TotalPrep RNA Amplification Kit. The hybridization was performed on Illumina Human-HT12 Version 4 arrays. Raw data exported from Illumina GenomeStudio were processed using the normexp algorithm, which applies non-parametric background correction using negative control probes, followed by quantile normalization with both negative and positive control probes. Gene expression values for replicated genes were aggregated using the median value.

In order to study the biological processes associated with the genes differentially down expressed in GEN2.2 shSIDT vs shCTL at steady state or after 6h of stimulation (log2 fold change < -1.5), we investigated the enrichment of functional annotations using the GeneCODIS tool,[36] which uses functional descriptors of biological processes to evaluate the annotations that are enriched in a gene list. Gene Ontology (GO) annotations for biological processes were considered significant when the adjusted hypergeometric p value (Hyp_c) < 0.01. Gene regulatory networks were explored using the ConsensusPathDB meta-database v33[37] (cpdb.molgen.mpg.de). The test gene set consisted in the genes significantly downexpressed in shSIDT1 vs shCTL GEN2.2 cells after 6h of ODN2006 stimulation (log2 fold decrease < -1.5; adjusted p value < 0.01). The intermediate nodes Z-score threshold was set at 10. Only genetic interactions were evaluated.

The gene co-expression search engine SEEK (http://seek.princeton.edu/) was used to find human genes co-expressed with SIDT1,[38] as well as to identify GO biological processes enriched in these gene sets. The algorithm was interrogated firstly for all datasets in the database and secondly for blood cell lines-related data sets, and finally for skin-related (non cancer) data sets.

Microscopy

Primary human pDC were collected after purification, fixed in 2% PFA for 15 min and stained with a rabbit polyclonal αSIDT1 antibody (Santa Cruz Biotechnology Cat# sc-67265, RRID:AB_2188887)[39] alone or in combination with a policlonal sheep αEEA-1 (R&D Systems, Cat# AF8047, RRID:AB_2893082) and a mouse monoclonal αLAMP1 (Millipore Cat# 428017, RRID:AB_2134501). Secondary antibodies were αrabbit conjugated with Alexa Fluor-488 (Thermo Fisher Scientific anti-rabbit Cat# A-11034, RRID:AB_2576217) and αsheep-Alexa Fluor555 (Thermo Fisher Scientific anti-sheep Cat# A-21436, RRID:AB_2535857) or αmouse-Alexa Fluor555 (Cat# A32727, RRID:AB_2633276). Similarly, GEN2.2, shCTL and shSIDT cells in steady state or after 1h of stimulation with 1 μM ODN2006 were collected and fixed in PFA 2% for 15 min. Afterwards they were immunostained with goat αTLR9 (Santa Cruz Biotechnology Cat# sc-16247, RRID:AB_2271834) and mouse αLAMP1 (Millipore Cat# 428017, RRID:AB_2134501) and goat αmouse-Alexa Fluor-555 (Thermo Fisher Scientific Cat# A32727, RRID:AB_2633276) and donkey αgoat Alexa Fluor 647 (Thermo Fisher Scientific Cat# A32849, RRID:AB_2762840) conjugated secondary antibodies. Nuclear staining was performed with 1 μM Hoechst 33342 (Sigma).

GEN2.2 cells stimulated with ODN2006 and ODN2216 were stainined with αSIDT1 antibody in combination with αEEA-1 or αLAMP-1.

HEK293 expressing TLR9-YFP and SIDT1-CFP were plated in 8-well slides coated with poly-L lysine (IBIDI). Cells were stimulated with 1 μM ODN2006 for different times at 37 °C.

For the *in vivo* labeling of acidic vesicles, GEN2.2 cells were cultured at a density of 4×10^6 cells/well in 96-wells flat plates (NUNC, ThermoScience Cat# 167008) and incubated in RPMI 1640 medium supplemented with 10% FBS containing 0.5 μM LysoTracker Red DND-99 (Life Technologies Cat# L7528) for 30 min at 37 °C. Afterwards, LysoTracker was washed off with medium, and the cells were incubated for 60 min in culture medium at 37 °C, to ensure the access of LysoTracker to the acidic vesicles. Finally, cells were stimulated with 0.1 μM ODN2006-Cy5 plus unlabeled ODN2006 or 0.2 μM ODN2216-Cy5 plus unlabeled ODN2216 (both from Life Technologies) to a final concentration of 1 μM at 37 °C.

Images were acquired on live cells using a laser-scanning confocal microscope system LSM 710 (ZEISS) with a camera of incubation at 37 °C of temperature and 5% CO2, using an oil-immersion objective (63X /1.40 Dec M27 numerical aperture). Co-localization analysis was carried out using the Zeiss ZEN software, by calculating the overlap coefficient, ranking from 0 to 1.[40] A value of zero means that there are no overlapping pixels. For GEN2.2 LAMP1/TLR9, SIDT-1/EEA-1 and SIDT-1/LAMP1 colocalization experiments overlap coefficient was calculated for individual cells with Zeiss ZEN software. In LAMP1/TLR9 co-localization assays a minimum value of 0.6 was fixed to consider positive. At least 100 cells from 3 independent experiments were counted and final number of positive and negative cells was represented. To evaluate colocalization of SIDT1 with EEA-1 and LAMP1 in GEN2.2 cells overlap coefficient was calculated for a minimun of 25 individual cells of at least two independent experiments.

Statistical analysis

For the animal model experiments, the sample size was chosen using Piface software,[41] retrieved from http://www.stat.uiowa.edu/~rlenth/Power. Outliers were detected using a two-side Grubbs' test and eliminated

from the analysis. Statistically significant differences between 2 groups were determined using two-tailed unpaired t test, Mann-Whitney, Wilcoxon U test, Chi square or Fisher exact tests when indicated. D'Agostino-Pearson test was used for normality distribution assessment. Graphs and statistical analyses were performed using the software Prism 9.0.0 (GraphPad Software Inc.) or SPSS 23.0 (IBM Spss Statistics). Values are reported as individual values, and plotted as mean ± SD, or as median and IQ range. Significant differences were assigned at a value of $p < 0.05$.

Study approval

All the experimental procedures in mice were approved by the Ethical committee of University of Granada and Consejería de Agricultura, Pesca y Desarrollo Rural, Junta de Andalucía (Protocol number 12/12/14/169). The protocols regarding pDC isolation from blood of healthy donors were approved by the Comité de Ètica de la Investigación (CEI/CEIM) of Granada, for the proposal PI18/00082). All the donors signed an informed consent form before sample donation.

Role of funders

Funding was obtained from the Consejería de Salud de la Junta de Andalucía (PIER_S1149 and C2_S0050) and Instituto de Salud Carlos III (PI18/00082 and PI21/01151), partly supported by European FEDER funds, and prior funding to MEAR from the Alliance for Lupus Research and the Swedish Research Council. Funders did not have any role in the study design, data collection, data analysis, interpretation, or writing of the report.

Results

SIDT1 is expressed in pDC and is induced by TLR7 and TLR9 ligands

Since it has been suggested that SIDT1 could have a role in the antiviral IFN-I responses,[26] we wondered about the role of SIDT1 in the main IFN-I producers, the pDC. Public gene expression data anotation portal BioGPS[42,43] revealed that SIDT1 mRNA is specifically expressed in the human lymphoid lineage including T and B lymphocytes, NK and pDC as previously shown in[26] (see http://biogps.org/#goto=genereport&id=54847). Additionally, the co-expression search engine SEEK revealed the enrichment of SIDT1-coexpressed genes in GO biological processes related to the immune response, and more precisely in IFN-I and cytokine-related processes (Table S1, sheets GO BP all datasets and GP BP blood cell lines). GEN2.2 cell line was chosen as a relevant pDC model to study the role of SIDT1 in the recognition of exogenous nucleic acids by endosomal TLR, since they share most of the phenotypic[17] and transcriptomic features[44] of circulating primary pDC.

As shown in Figure 1a, SIDT1 is expressed in both, primary pDC and in GEN2.2 cell line showing an identical distribution pattern. TLR7 (resiquimod) and TLR9 (ODN2006) stimulation upregulated the expression of SIDT1 in the pDC cell line GEN2.2 (Figure 1b). Similar results were obtained in the pDC line PMDC05 (laboratory data), as well as in primary pDC (Figure 1c). Such expression induction suggests that SIDT1 could be involved in the response to endosomal TLR in pDC.

SIDT1 silencing leads to the downward expression of IFN-related genes

We silenced SIDT1 in GEN2.2 combining three polycistronic shRNA vectors expressing GFP (Figs. S1a and S1b), achieving a reduction of SIDT1 expression by 60% at the RNA and protein levels (Figs. S1c and S1d). Gene expression array experiments were carried out in ODN2006-stimulated GEN2.2 shSIDT1 cells at different time points as in.[44] The most prominent transcriptional differences were obtained after 6 h of stimulation. As shown in Table S2, (sheet shSIDT1 vs shCTL), 436 genes were significantly underexpressed in shSIDT1 cells (adjusted $p < 0.01$) compared with shCTL cells at T0, and 831 genes at 6h. Among them, we selected those with a log2 fold change < -1.5 ($n = 64$ and $n = 60$, for T0 and 6 h, respectively). The analysis of the biological processes associated with these genes using GeneCodis[36] revealed that 4 out of the 6 most significant downregulated pathways in resting cells were involved in the immune response (Table S2, sheet T0 biological processes). Accordingly, a repression of immune response-related biological processes was also significantly associated with the transcriptional profile of ODN2006-stimulated shSIDT1 cells (Table S2, T6h biological processes). The genes included in the most significant categories were mainly chemokines, IFNα/β and IFN-dependent molecules.

In order to dissect the gene regulatory interactions that underlie the differential gene expression profiles in CpG-stimulated shSIDT1 cells, we used the ConsensusPathDB meta-database v30,[37] selecting the genes with a log2 fold change shSIDT1/shCTL < -1.5 and $p < 0.01$ as before. As shown in Figure 1d, the major regulatory network defined by the algorithm was related with the IFN-I responses, with the most connected genes being IFN-I molecules (i.e. *IFNB1*), transcription factors involved in the induction of IFN responses (*IFR2, IRF3, IRF7*) and IRF-dependent chemokines (*CXCL9, CXCL10, CXCL11*). Other chemokines were dependent on both IRFs and NF-κB (*CCL3, CCL3L1, CCL3L3*). All together, our results suggest that SIDT1 silencing could affect primarily the IRF-mediated IFN-I response pathway in human pDC after TLR9

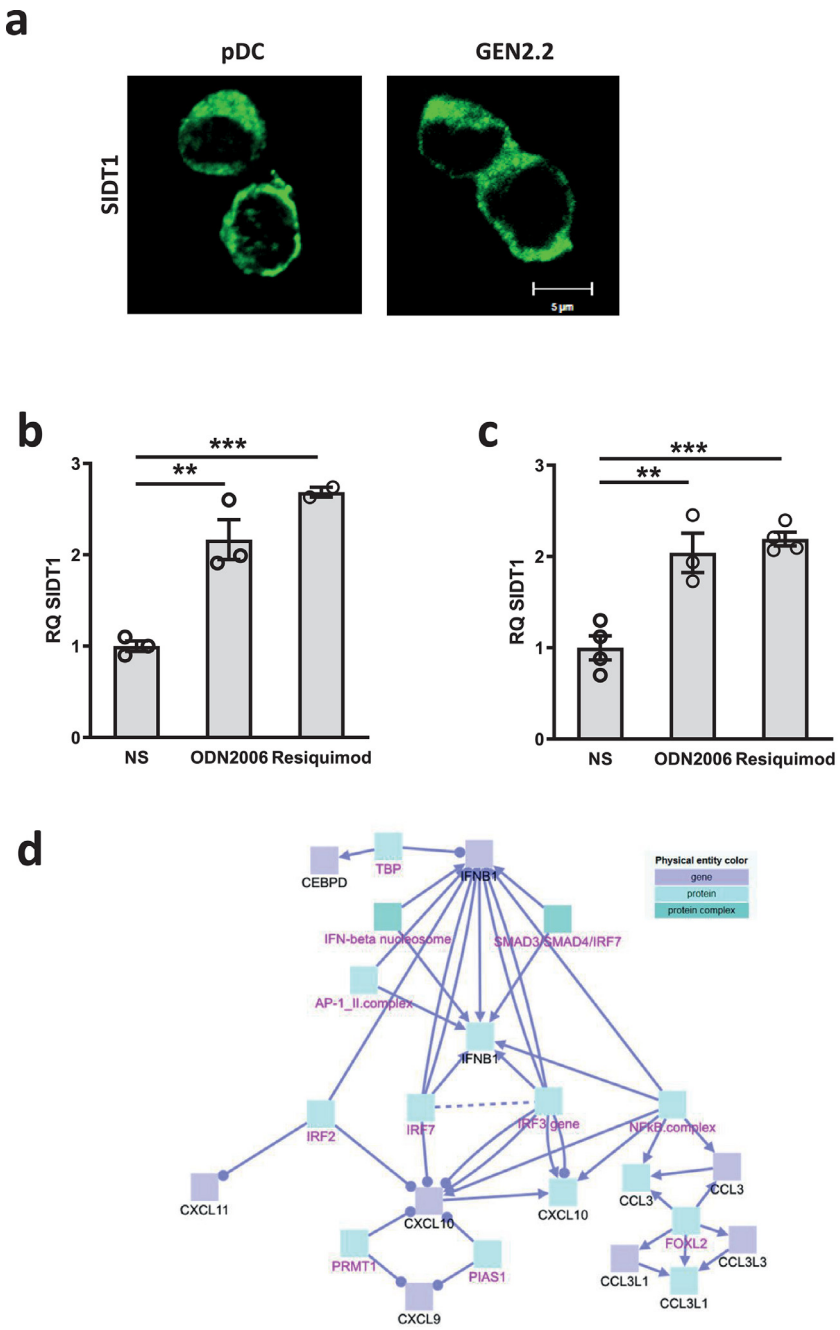

Figure 1. SIDT1 is expressed in pDC and induced by TLR7 and TLR9 ligands. **(a)** SIDT1 detection in primary human pDC (left panel) and GEN2.2 cells (right panel) by immunofluorescence. **(b)** *SIDT1* mRNA quantification in GEN2.2 cells stimulated with ligands of TLR9 (ODN2006) and TLR7 (resiquimod) using dPCR. Mean and standard deviation values are plotted. **(c)** *SIDT1* mRNA quantification in human pDC after stimulation *ex vivo* with ODN2006 and resiquimod as in (b). Data shown in (a) and (b) are representative of at least four experiments, samples were tested in triplicates. ** $p < .01$; *** $p < .001$ in two tailed t-student tests. **(d)** SIDT1 underexpression leads to the downward expression of IFN-related genes in GEN2.2 cells. Gene regulatory interaction analysis of SIDT1-silenced GEN2.2 cells. Top down-regulated genes in GEN2.2 shSIDT1+CpG (6h) relative to shCTL+CpG were used to dissect the gene regulatory interactions where SIDT1 is involved. This figure was prepared using ConsensusPathDB as described in Methods. Black legends denote seed nodes. Purple legends denote intermediate nodes. Arrows denote a substrate/product interaction and circles denote enzyme interaction. In the context of genetic interaction networks both edge types are equivalents and the choice depend on the notation of the different data bases interrogated. Continous line denotes activation. Discontinous line denotes inhibition.

stimulation, in agreement with the transcription factor analysis carried out using GeneCodis (Table S2, sheet TF 6 h).

SIDT1 is specifically involved in type I and III IFN responses, but not in pro-inflammatory cytokine responses

Next, we monitored the cytokine secretion profile of shSIDT1 GEN2.2 cells after endosomal TLR stimulation. As expected, the secretion of the proinflammatory cytokines TNFα, IL-6, and IL-8 after TLR7 (imiquimod) and TLR9 (ODN2006) stimulation was barely affected in shSIDT1 cells (Figure 2a), as well as the expression of surface activation markers (Figure 2c). Interestingly, the production of IFNα was greatly impaired in shSIDT1 cells after TLR9 stimulation with type-A (ODN2216) and type-B (ODN2006) CpG oligonucleotides, as well as after TLR7 stimulation with imiquimod and resiquimod (Figure 2b). The secretion of the type III IFN molecule IL-29 (IFNλ1) and the IFN-dependent chemokine CCL3/MIP-1α was also inhibited after stimulation (Figure 2b) in agreement with the previous RNA expression array results.

We silenced *SIDT1* in BDCA4$^+$ pDC from blood of healthy donors (Figure S2a). Since primary human pDC are difficult to transduce and maintain *in vitro*, pDC were immediately transduced *ex vivo* with shSIDT1 lentiviral particles, and simultaneously stimulated with ODN2006 for 18 h. As shown in Figure S2b, this protocol induced a low-to-moderate expression of GFP, and a decrease of around 40% in *SIDT1* mRNA. Although the silencing effect was modest, the effect on the IFN-I response to ODN2006 stimulation was remarkable, since a 3-log inhibition of IFN-I expression was observed, while the TNFα response was preserved (Figure 2d), indicating that SIDT1 is selectively mediating IFN-I but not in proinflammatory pathways in human pDC. shSIDT1 GEN2.2 cells also showed a poor type I IFN secretion after stimulation of cytosolic DNA sensors (Figure 2e, lipo+ODN). These results indicate that SIDT1 is not exclusively involved in the activation of canonical endosomal receptors such as TLR7 and TLR9, but also acts in the cytosolic sensing pathway. However cytosolic dsRNA sensors were not affected in shSIDT1 cells (Figure 2e, lipo+polyI:C). GEN2.2 cells did not respond to polyI:C stimulation, in agreement to the absence of TLR3 in pDC[45] and GEN2.2 (laboratory data). GEN2.2 cells also reacted to the stimulation of cytosolic nucleic acid sensors with the secretion of proinflammatory cytokines such as TNFα. As it was shown above for endosomal receptors, TNFα responses were not affected by SIDT1 silencing (Figure 2e, TNFα panel). *C. elegans* SID-1 protein but not ChUP-1 ortholog would mediate passive entry of extracellular RNAi.[46] Additionally, human SIDT1 shows very low affinity for short length dsRNA or DNA.[47] Accordingly, we could not observe a significant inhibition in the entry of ODN2006-Cy5 in shSIDT1 cells, in agreement with[26] (Figure S3a). Indeed, the defective IFN-I response of shSIDT1 GEN2.2 cells was not restored adding more ODN2006 (Figure S3b, top panel), and the TNFα response was comparable in shSIDT1 and control cells at all doses tested (Figure S3b, bottom panel). Of note, the expression of the genes *TLR7* and *TLR9* were not repressed in shSIDT1 cells (Table S2 and laboratory data). Altogether, our data indicate that the skewed IFN-I responses in shSIDT1 cells are not due to a defect in the transport of exogenous nucleic acids into the cell or to a lower expression of TLR7/9. Additionally, ODN2006-induced IFN-I responses in WT GEN2.2 showed a maximum at 24h, whereas the response to imiquimod was the highest around 48–72 h (see Figure S3c). The IFN-I responses observed in shSIDT1 cells followed the same kinetics but had a much lower intensity. Similar results were obtained using other TLR7 and TLR9 stimulators, such as resiquimod and ODN2216 (laboratory data). Thus, our data indicate that SIDT1 silencing does not induce a delay in the IFN-I responses, but a true inhibition.

SIDT1 is involved in the access of TLR9 and CpG to endolysosomal vesicles

It was reported that SIDT1 expressed ectopically in HEK293 cells is located in cholesterol-rich domains in the RE and translocates to intracellular vesicles and the cell membrane in cholesterol reduced conditions.[23] Thus, we studied the distribution of SIDT1, and its dynamics after ODN2006 stimulation of TLR9. Similarly, TLR9 is also located in the ER in steady state and mobilizes to intracellular vesicles after stimulation.[13] Therefore, confocal co-localization experiments were carried out using HEK-293 expressing both SIDT1-CFP and TLR9-YFP. In these cells TLR9-YFP is functional, since transfected cells secreted IL-8 after ODN2006 stimulation, but not in the absence of the TLR9-YFP vector (laboratory data). In resting cells, the confocal images show SIDT1 mostly co-localizing with TLR9 in the ER (Figure 3a, NS). Both TLR9 and SIDT1 were mobilized after ODN2006 stimulation and co-localized in vesicles and in a minor extent to the plasma membrane (Figure 3a, ODN2006), indicating that SIDT1 is located together with TLR9 in the ER in steady state, and that both molecules co-migrate to intracellular vesicles after stimulation.

In order to characterize the vesicles containing SIDT1 after stimulation we performed some co-localization experiments. GEN2.2, shCTL and shSIDT1 cells were stimulated with ODN2006 and ODN2216 for 1 h. Afterwards the cells were stained for SIDT1 in combination with markers for early endosomes (EEA-1; Figure 3b) and lysosomes

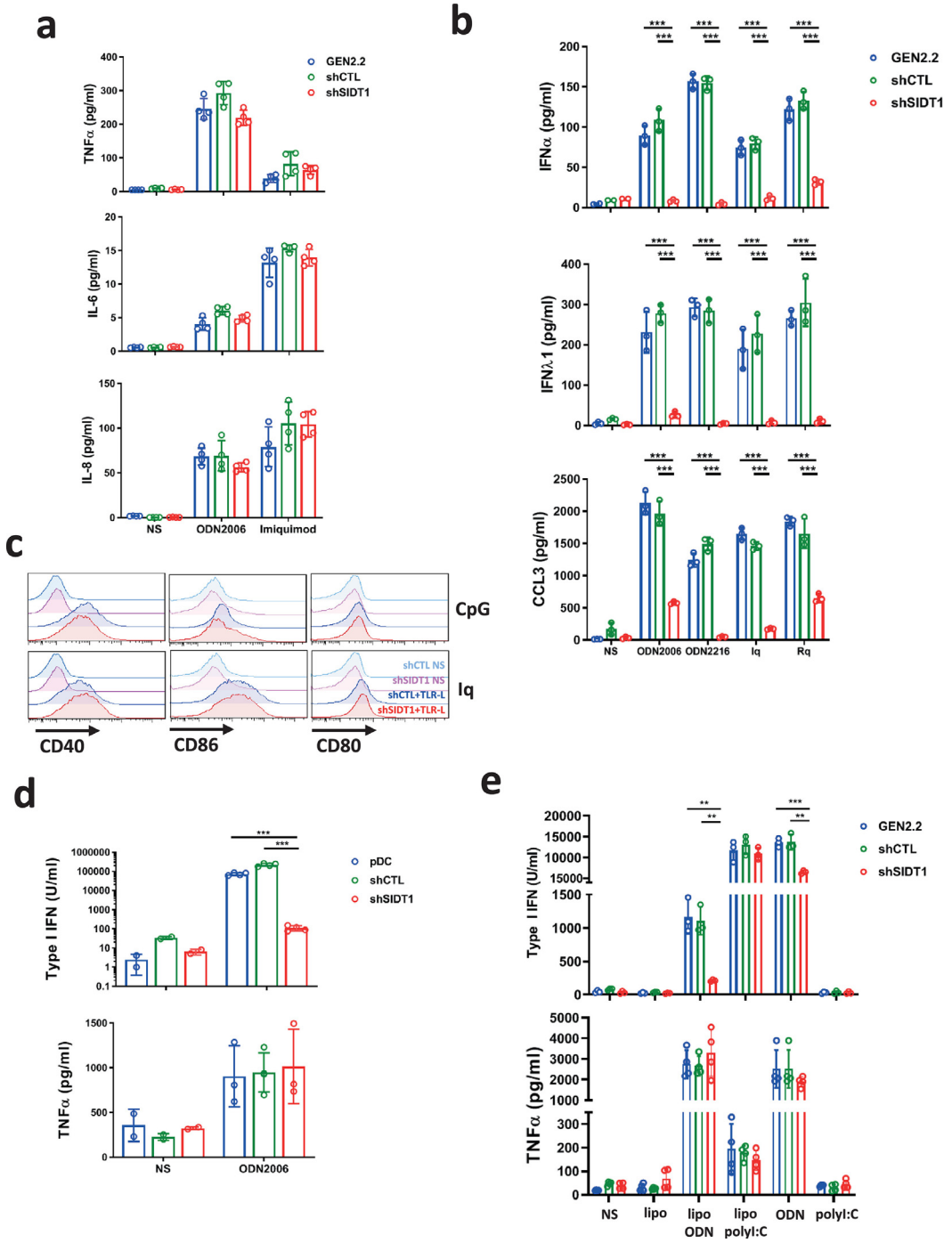

Figure 2. SIDT1 is involved in type I and III IFN, but not in proinflammatory cytokine responses. **(a)** Secretion of proinflammatory cytokines by SIDT1-silenced GEN2.2 cells and their controls after 24 h of stimulation. **(b)** Quantification of IFNα, IFNλ1 (24h) and CCL3 (8h) in the supernatants of shSIDT1 GEN2.2 cells and their controls after stimulation with ligands of TLR9 (ODN2006 and ODN2216) and TLR7 (Imiquimod, Iq and resiquimod, Rq). **(c)** GEN2.2 shCTL and shSIDT1 cells were stimulated with ODN2006 (CpG) and imiquimod (Iq) for 24 h and the surface expression of costimulatory molecules was measured by flow cytometry. **(d)** Detection of type I IFN and TNFα in the supernatants of primary shSIDT1 pDC stimulated with ODN2006. **(e)** Cytokine responses of GEN2.2 shSIDT1 and control cells after stimulation of cytosolic receptors of DNA (CpG+lipofectamine) and RNA (polyI:C+lipofectamine). Lipofectamine alone and ligands in absence of lipofectamine were included as controls. Supernatants were analyzed after 24 h of stimulation. Top panel, Type I IFN; bottom panel, TNFα. The data shown are representative of at least five independent experiments for GEN2.2 (a, b, c and e) and of four experiments for pDC (d). ** $p < .01$ *** $p < .001$ in t-student tests.

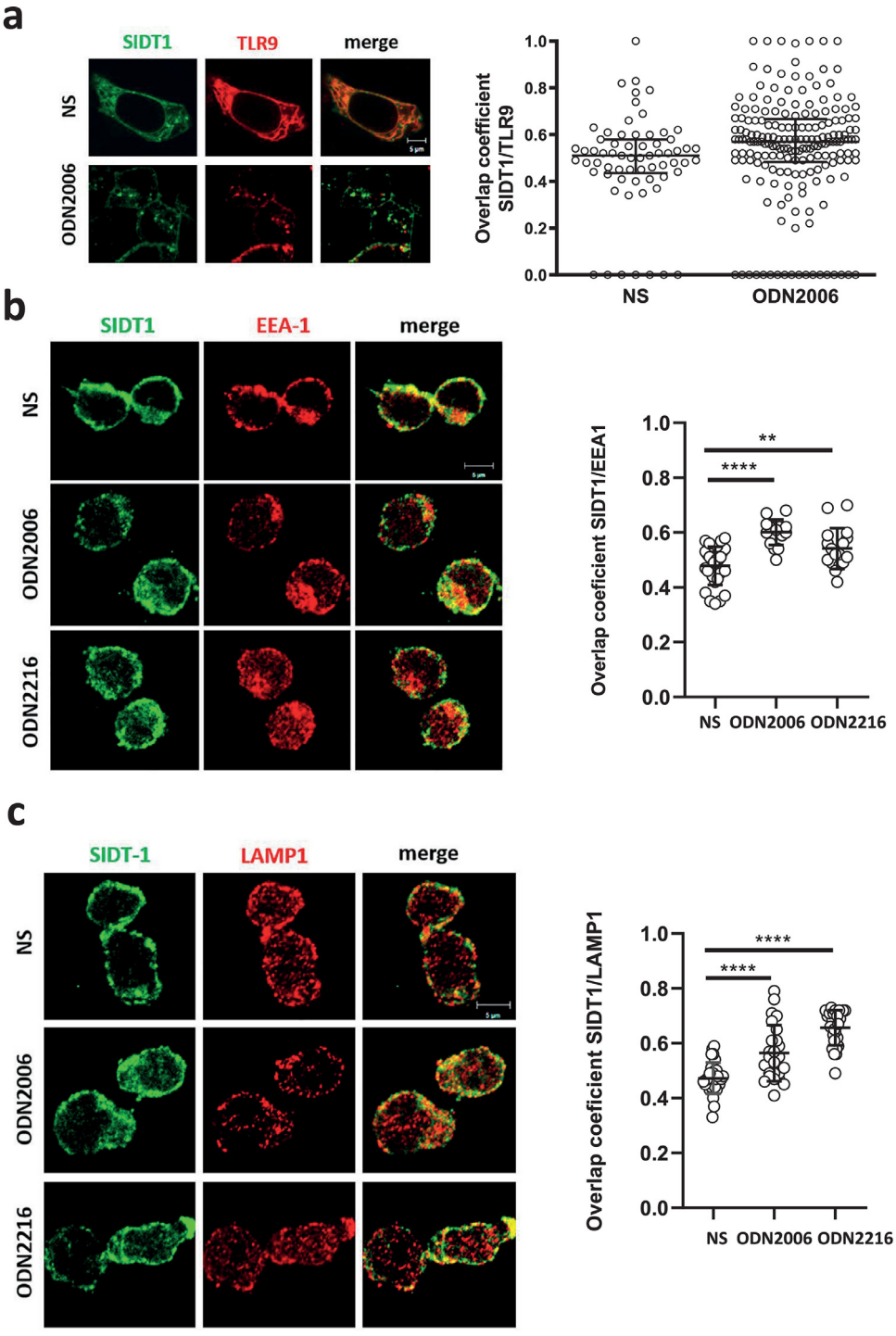

Figure 3. Intracelular localization of SIDT1 in resting and stimulated cells. **(a)** Confocal microscopy images of SIDT1-CFP and TLR9-YFP in HEK cells before and after ODN2006 stimulation (18h). Left, representative results: right, quantification of SIDT1-TLR9 co-localization using two independent experiments. **(b)** Colocalization of SIDT1 with the early lysosomal marker EEA-1 in GEN2.2 before (NS) and after stimulation for 1h with ODN2006 and ODN2216. Left panel, representative images. Right planel, quantification of overlap coefficient using two independent experiments and a minimun of 25 cells per condition. **(c)** Colocalization of SIDT1 with the lysosomal marker LAMP1 as in (b). Individual values, mean and standard deviation values are plotted. **** $p < 0.0001$; ** $p < 0.01$ in t-student tests.

(LAMP1; Figure 3c). We corroborated that SIDT1 colocalized partially with both markers in steady state, and that it is mobilized after ODN2006 and ODN2216 stimulation, increasing colocalization coefficients with both EEA-1 and LAMP1. This data indicate that SIDT1 is mobilized to early endosomes and lysosomes after TLR9 stimulation. A similar co-localization pattern was observed in primay pDC (Figure S4a).

The NF-kB-dependent induction of proinflammatory cytokines and co-stimulatory molecules is initiated upon ligation of intracellular TLR with their ligands in the endosomal compartment in pDC. The vesicles containing the TLR/TLR-L complexes can also translocate to an acidic compartment, where IRF7-dependent IFN-I pathway is initiated.[16,21] Therefore, we evaluated the access to the endolysosomal compartment of TLR9 in shSIDT1 GEN2.2 cells after stimulation. 4 h after stimulation there was a significant increase in the number of cells in which TLR9 was translocated to endolysosomal vesicles expressing LAMP1 in WT and shCTL GEN2.2 cells as in.[17] However, in shSIDT1 GEN2.2 cells we could not observe any increase in TLR9/LAMP1 colocalization (Figure 4a). Confocal studies using the fluorescent TLR9 ligand ODN2006-Cy5 evidenced that ODN2006 reached to acidic vesicles after 1h of incubation in WT and shCTL GEN2.2, revealed by a positive co-localization signal in LysoTracker-labeled vesicles. Interestingly we obtained significantly lower numbers of cells showing co-localization between ODN2006-Cy5 and LysoTracker in shSIDT1 GEN2.2 (Figure 4b). Similar results were obtained using ODN2216-Cy5 (Figure S4b). Altogether, our results indicate that SIDT1 plays a relevant role in the access of TLR9-CpG complexes to the acidic vesicular compartments, where IFN-I signaling is initiated.[15]

SIDT1 is required for the nuclear translocation of IRF7 but not of NF-κB

The TBK1/IKKε complex has a central role in the transduction cascade resulting in the induction of IFN-I after TLR7 and TLR9 stimulation, since it phosphorylates several members of the IRF family, inducing their translocation to the nucleus.[48,49] As shown in Figure 5a, TLR9 stimulation of shSIDT1 cells failed to correctly induce a proper phosphorylation of TBK1, otherwise clearly visible in control cells (GEN2.2 and shCTL). Since IRF7 is a key factor for IFN-I responses in pDC,[50] we tested the translocation of IRF7 to the nucleus after stimulation of TLR7 and TLR9. The nuclear translocation of IRF7 was impaired in shSIDT1 cells (Figure 5b and S5a). Moreover, western blot analysis showed more pronounced increase of the induction of the phosphorylated form of IFR7 in GEN2.2 and shCTL compared with shSIDT1, detected as a band with a lower electrophoretic mobility in the nuclear fraction (higher apparent molecular weight).[51] On the other hand, the nuclear translocation of the NF-kB p65 protein after stimulation was not inhibited in shSIDT1 cells, as assessed by image cytometry (Figure 5b), and even showed an increase in western blot analyses (Figure S5b), probably due to a compensatory mechanism or a longer endosomal persistence of the TLR9-NF-kB compex. The conserved translocation of NF-κB p65 in shSIDT1 cells agrees with the unchanged profile of proinflammatory cytokine secretion and costimulatory proteins shown previously (Figure 2).

Overall, our results indicate that SIDT1 is required for the correct signaling cascade involved in the induction of IFN-I in human pDC, but not the proinflammatory responses, through the control of the phosphorylation of TBK1, and the nuclear translocation of IRF7.

SIDT1 is mediating IFN-I responses to endosomal TLR in mouse pDC

We took advantage of *sidt1*$^{-/-}$ mice, generated through the deletion of exons 2-3 in C57BL/6 strain.[26,29] As expected, splenocytes of *sidt1*$^{-/-}$ animals produced low amounts of IFN-I in response to TLR7 (imiquimod and resiquimod) and TLR9 stimulation (ODN2216), while TNFα responses were preserved in all cases (Figure 6a). Moreover, bone marrow-derived pDC (BM-pDC) from *sidt1*$^{-/-}$ mice were also poor producers of IFN-I in response to CpG compared to those of WT animals, while the TNFα responses and the overexpression of maturation markers were similar to WT (Figure 6b). In agreement with our previous observations using human cells, the absence of SIDT1 in mouse pDC had a strong effect in IFR7 nuclear translocation after TLR7 and TLR9 stimulation with resiquimod and ODN2216, respectively, while preserving NF-κB translocation (Figure 6c). Thus, these data indicate that SIDT1 is also mediating IFN-I responses to endosomal TLR in mouse pDC.

SIDT1 deficiency ameliorates TLR7-mediated psoriasis-like dermatosis murine model

Interestingly, when SEEK tool was used to explore SIDT1-coexpressed genes in skin-related data sets, psoriasis-related samples were ranking on the top of the list (see table S1, spreadsheet skin datasets). Therefore, since the imiquimod-induced psoriasis-like acute dermatitis model is highly dependent on the IFN-I responses,[34,52,53] we tested the outcome of *sidt1*$^{-/-}$ mice after topic imiquimod (Aldara cream) treatment.[54] First of all the IFN-I levels in serum of aldara-treated *sidt1*$^{-/-}$ mice were significantly reduced compared to WT animals, while no difference was observed in TNFα levels,

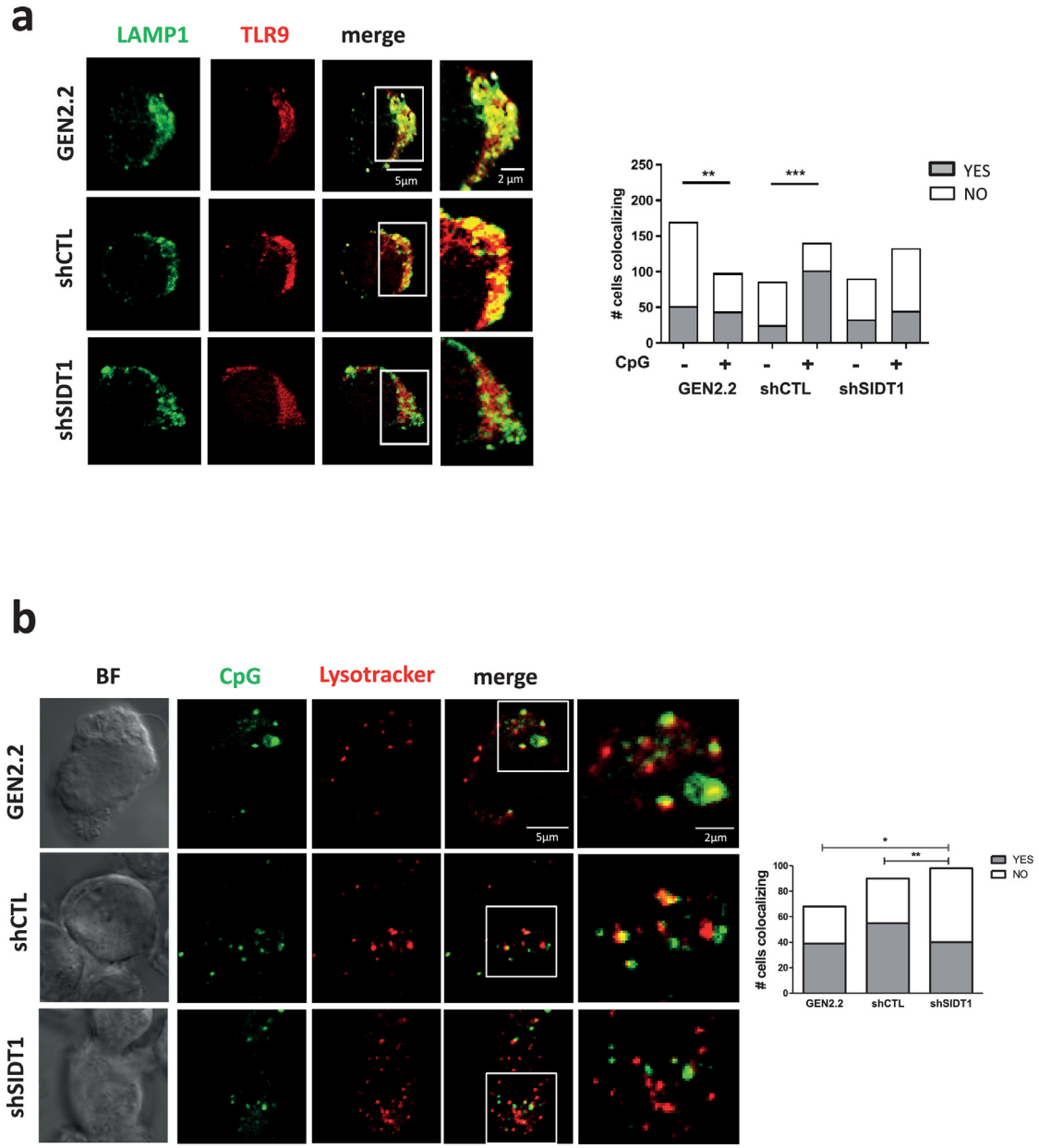

Figure 4. SIDT1 is involved in the lysosomal trafficking of CpG-TLR9 complexes. **(a)** Colocalization of TLR9 and the lysosomal marker LAMP1 in GEN2.2, shCTL and shSIDT1 cells after 4h of stimulation with ODN2006. Left panel, representative images of stimulated cells. Right panel, quantification of cells showing TLR9-LAMP1 colocalization before and after CpG (ODN2006) stimulation. **(b)** Lyso-Tracker red-labeled cells were incubated with ODN2006-Cy5 for 1h and visualized by live cell imaging. Left, representative confocal microscopy images. Right, quantification of cells showing ODN2006/LysoTracker colocalization. *$p < .05$, ** $p < .01$, *** $p < .001$ using a Fisher's exact tests. The results shown are representative of at least two independent experiments.

indicating that the pro-inflammatory branch of TLR7 pathway remains active (Figure 6d).

Following 6 days of treatment, SIDT1-deficient mice demonstrated improved macroscopical disease scores as compared to WT animals accompanied with reduced splenomegaly, indicating a less severe disease expression (Figure 7a). The histological analysis revealed a reduction in keratosis and apparent pseudo-papillomatosis measured through the keratine surface and the suprapapular thickness, respectively, in *sidt1*$^{-/-}$ mice. In addition, the number of animals presenting pustules of Kogoj was significantly lower (Figure 7b).

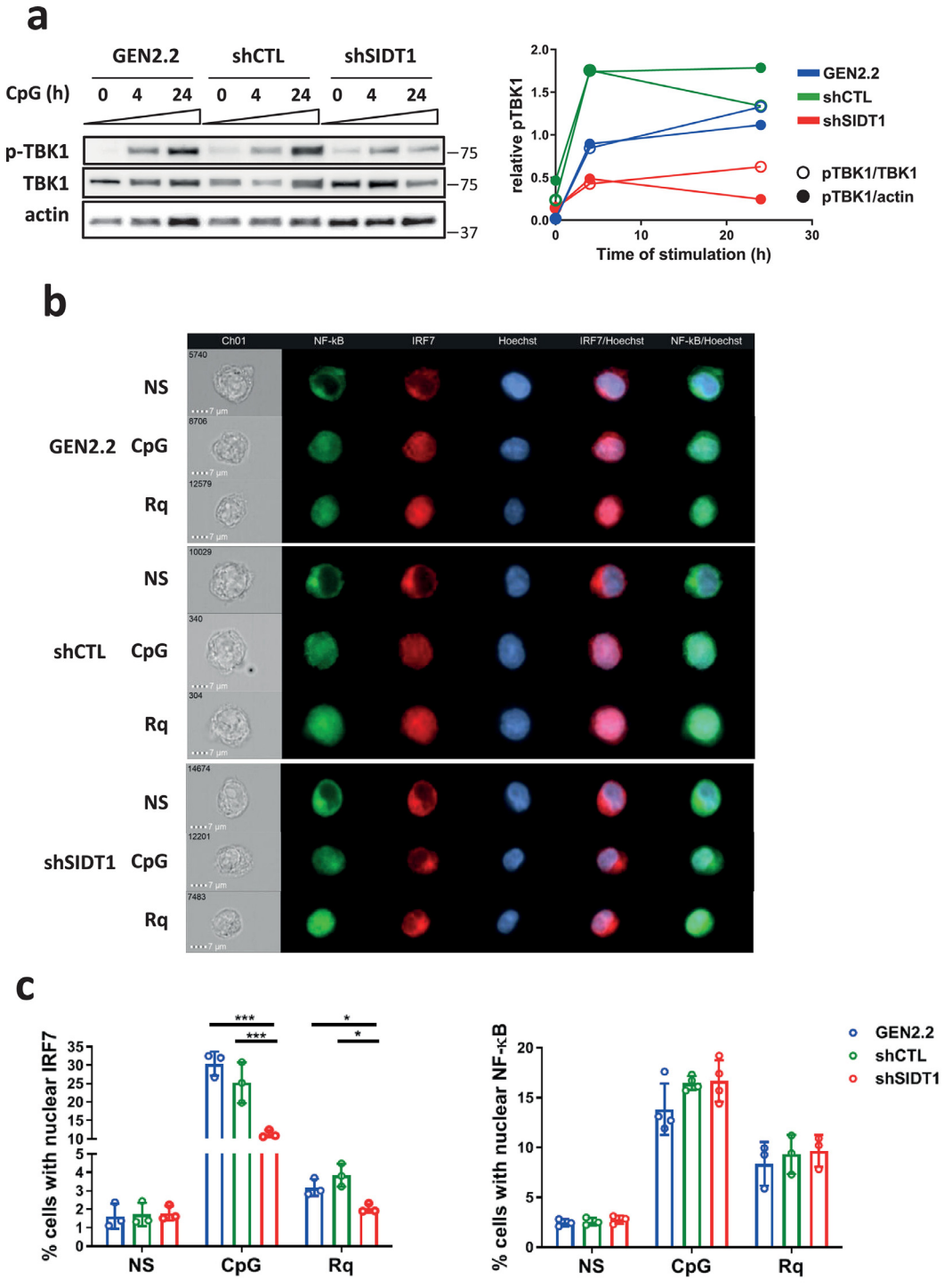

Figure 5. SIDT1 is required for the activation of the TBK1/IRF7 cascade, but not for the NF-κB pathway. SIDT1-silenced GEN2.2 cells and their controls were stimulated with 1 μM ODN2006 for the indicated time. **(a)** Cytosolic protein extracts were blotted against phosphorylated and total TBK1. p-TBK1/TBK1 intensity ratios are indicated. Actin was included as a loading control. Left panel, representative blots. Right panel, quantification of pTBK1/TBK1 and pTBK1/actin ratios from the blots. Full blots and MW markers are provided as supplementary material. **(b)** IRF7 and NF-κB nuclear translocation after stimulation with 1 μM ODN2006 (CpG) or 3 μg/ml resiquimod (Rq) of shSIDT1 GEN2.2 and control cells, monitored by image cytometry (representative images). **(c)** Quantification of the results. Individual values, mean and standard deviation values are plotted. The results are representative of at least three independent experiments with at least 10.000 acquired cells each. * $p < .05$, *** $p < .001$ using unpaired parametric t student's tests.

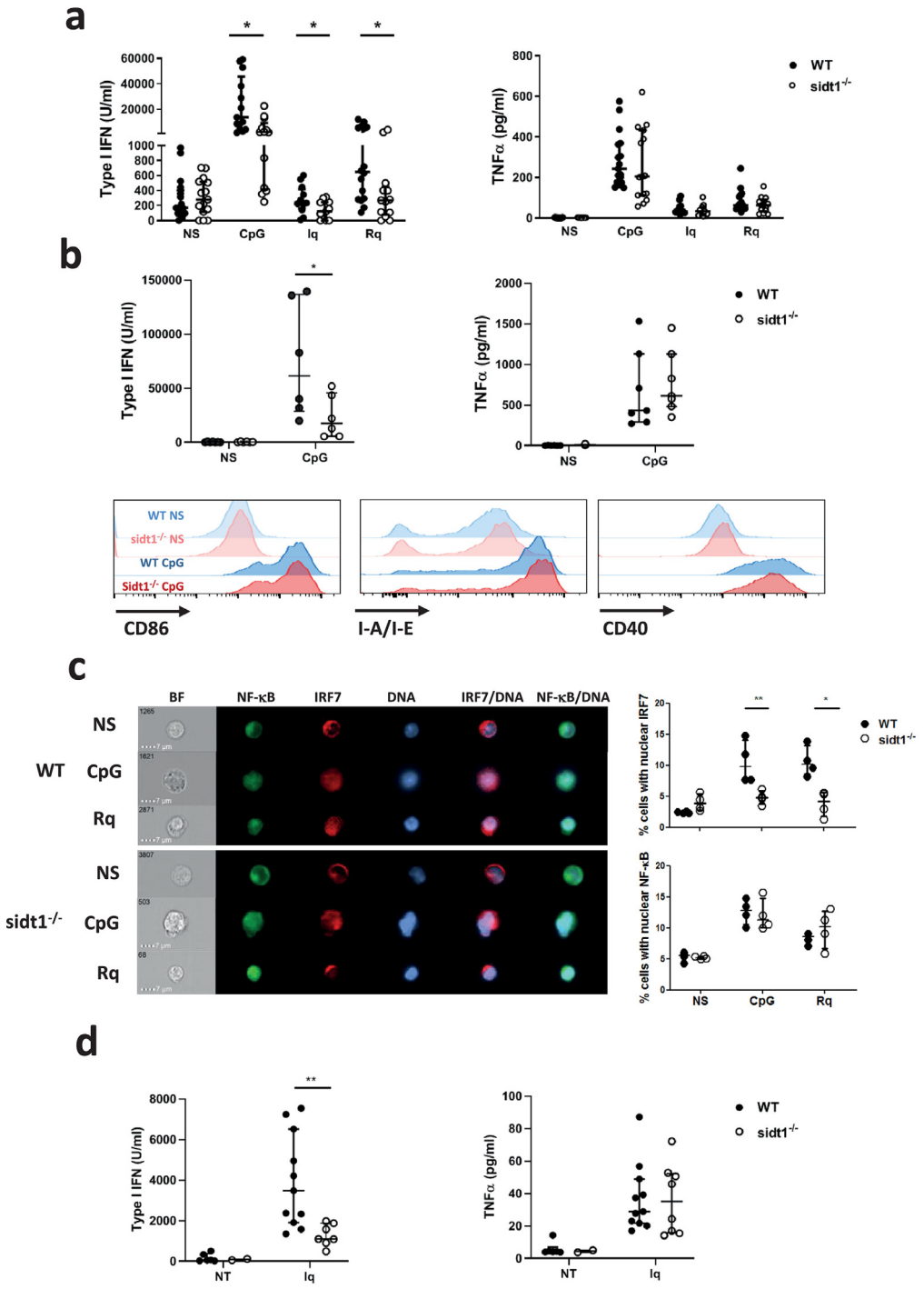

Figure 6. SIDT1 is mediating IFN-I responses to endosomal TLR in mouse pDC. **(a)** Splenocytes from WT ($n = 17$) and *sidt1*$^{-/-}$ ($n = 15$) mice were stimulated with ODN2216 (CpG), imiquimod (Iq) and resiquimod (Rq). Supernatants were collected at 48 h and assayed for type I IFN and TNFα. NS, non-stimulated **(b)** BM-pDC from WT ($n = 7$) and *sidt1*$^{-/-}$ ($n = 6$) mice were stimulated for 48h with ODN2216. Top panel, IFN-I and TNFα were quantified as before. Bottom panel, expression of maturation markers monitored by flow cytometry in the SiglecH^{+} gate, after exclusion of dead cells using DRAQ7. **(c)** BM-pDC were stimulated as in (b) and the translocation of NF-κB and IRF7 was quantified by image cytometry as in Figure 5. **(d)** Left, IFN-I levels in the serum of WT ($n = 11$) and *sidt1*$^{-/-}$ ($n = 8$) in untreated (NT) and Aldara (Iq) animals 2 h after treatment. Right, TNFα in serum of the same animals. Pooled animals of at least three independent experiments for (a) and (d) and two independent experiments in (b) and (c). Individual mice data, median and IQR values are plotted * $p < .05$; ** $p < .01$ in two-tailed Mann-Whitney tests.

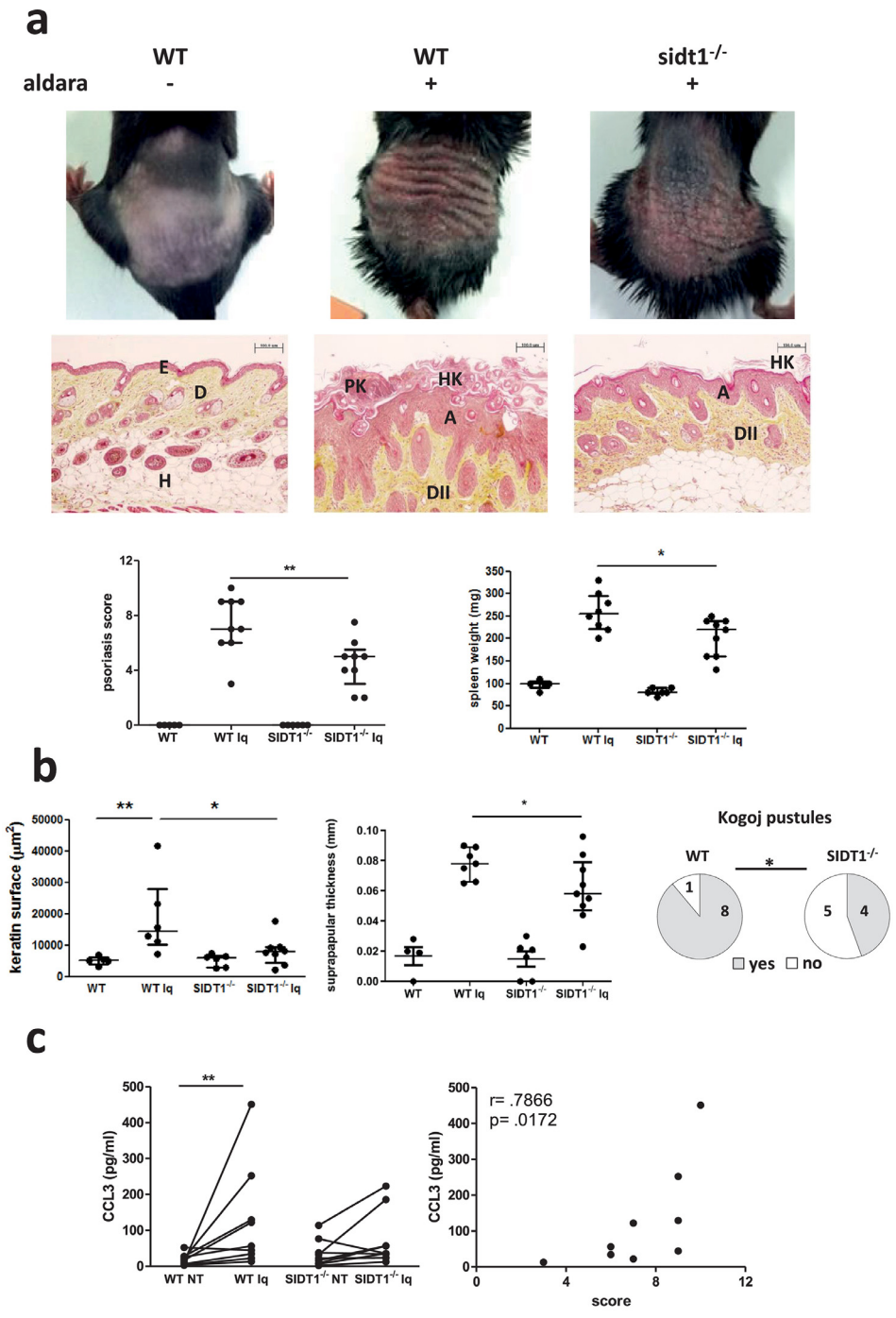

Figure 7. Improved outcome of psoriasis in *sidt1*$^{-/-}$ mice. WT and *sidt1*$^{-/-}$ mice were treated with placebo (Vaseline, NT) or Aldara cream (Iq) for 6 days. **(a)** Evaluation of the skin injury. Top panel, images of the back of the mice. Middle panel, histology of the skin of the same animals. E, epidermis; D, dermis; H, hypodermis; A acanthosis; DII dermal infiltrates; HK, hyperkeratosis; PK spongiform pustules of Kogoj. Bottom panels, psoriasis score and spleen weight. **(b)** Quantification of the keratin area and papillomatosis (through papula thickness measurement). Right, quantification of treated mice presenting Kogoj pustules lacking the granular layer. **(c)** CCL3 protein detection in paired samples of untreated (NT) and Aldara-treated (Iq) skin . Right, correlation between CCL3 levels in the skin and psoriasis score in WT mice using a Spearman test. Mice were pooled from three independent experiments. WT NT, $n = 5$; WT Iq, $n = 9$; *sidt1*$^{-/-}$ NT, $n = 6$, *sidt1*$^{-/-}$ Iq, $n = 9$. * $p < .05$, ** $p < .01$ in Mann-Withney tests. For Kogoj pustules analysis * $p < .05$ in Fisher test.

We also studied the local responses in the skin through the measurement of the concentration of 36 cytokines and chemokines. Our data evidenced an important increase in the IFN-dependent chemokines MIP1α (CCL3), IP-10, GROα, and MIP-2 in the treated skin compared with the untreated skin of the same animals in WT, but not in the *sidt1*$^{-/-}$ mice (Table S3). Of note, skin concentration of MIP1α/CCL3 showed a positive correlation with the severity score of the disease in WT mice (Figure 7c), as suggested before by.[55,56] As mentioned previously, a decrease of CCL3 production was also detected in shSIDT1 GEN2.2 cells (Figure 2c). Overall, from our data, SIDT1 mediates IFN-I responses *in vivo*, and is mediating pathological responses, in a TLR7-mediated psoriasis model.

Discussion

pDC are key players in the recognition of invading pathogens through their nucleic acid sensors and they produce balance quantities of proinflammatory cytokines and IFN-I. However in some pathological conditions this balance is broken, leading to the overproduction of IFN-I by pDC after stimulation by endogenous nucleic acids and immune complexes, and causing autoimmune and autoinflammatory disorders such as psoriasis.[3,57] Consequently, there is regained interest in the identification of novel players involved in the induction and control of the IFN-I and inflammatory responses by human pDC. It has been recently described that *sidt1*$^{-/-}$ mice are defective in the generation of antiviral IFN-I responses *in vivo*, showing normal TLR3-mediated IFN-I responses. As TLR3 ligands induce IFN-I responses in myeloid cells (monocytes/macrophages and conventional DC), it is likely that this defect is due to an impairment of the professional IFN-producing cells, the pDC, which are key in the orchestration of the proinflammatory/IFN balance after viral infection.[58,59]

Activation of nucleic acid-specific TLR triggers the activation of the transcription factors NF-κB and IRFs to promote pro-inflammatory and anti-viral IFN-I responses, respectively.[60] The regulation of receptor trafficking and localization is a critical parameter for these responses. TLR7 and TLR9 traffic follows the conventional secretory pathway from the ER to the Golgi, and then to the endosomal network through the plasma membrane.[61] The signals leading the transcriptional induction of two classes of genes (proinflammatory or alternatively type I and III IFN) originate from different types of endosomal vesicles,[50] and therefore the location of TLR7/9 and their ligands determines the precise outcome after pDC stimulation.[21] While the signaling in the late endosomes activates NF-κB and proinflammatory cytokines leading to a full maturation state, trafficking from endosomes to lysosome-related organelles is critical for IRF-dependent IFN gene expression.[15,62,63] The need of endosomal acidification for proper IFN-I responses is supported by the known inhibition of IFN-I responses by drugs that increase the lysosomal pH, such as chloroquine.[19,64] From our data, SIDT1 would mediate the traffic of the endosomal TLR-ligand complexes towards lysosomal-related organelles to activate IRF7 signaling, and inducing the IFN-I and IFN-III responses. Accordingly, we show defective TBK1 phosphorylation together with poor IRF7 nuclear translocation in both shSIDT1 GEN2.2 and mouse BM-pDC from *sidt1*$^{-/-}$ mice, while the NF-κB pathway was preserved. Mediators of the IRF pathway are promising drug targets for IFN-mediated and IRF-dependent diseases,[65] including TBK1.[49,66]

From our data, the involvement of SIDT1 in IFN-I production in response to exogenous nucleic acid stimulation is not restricted to TLR responses, however SIDT1 is not universally involved in all the IFN-I responses. SIDT1 silencing blocked IFN-I responses after the stimulation of cytosolic sensors of DNA but not dsRNA in GEN2.2. The role of intracellular vesicles in the cytosolic DNA recognition is not fully understood, however it has been proposed that communication between the lysosomal compartment and the cytosolic DNA sensors exists.[67,68] Furthermore, the exact location of the organelle hosting the TBK1 signalosome after cytosol DNA recognition in hematopoietic cells is still an open question.[69]

A tight regulation of cholesterol content and location is important for correct TLR responses,[70] primarily for IFN-I production.[71] Indeed, the recruitment of IRAK1 and TRAF6 to cholesterol-rich lipid bodies is required to induce the nuclear translocation of IRF7 after TLR7 and TLR9 stimulation in mouse pDC.[72] It is noteworthy that SIDT1 has a functional cholesterol-binding motif[22] and co-localizes with cholesterol in intracellular compartments,[23] pointing to a role for SIDT1 in the traffic of cholesterol-rich membranes. Additionally a role for *C. elegans* ChUP-1 ortholog in the uptake of dietary cholesterol[23] and in the generation of a protective innate response has been recently reported,[24] linking cholesterol metabolism and the immune response. In this line a recent study reported that SIDT1 is expressed in the gastric pit cells of the stomach, being involved in the absorption of dietary microRNAs.[29] Of note, exogenous microRNA encapsulated into cholesterol-rich exosomes has been shown to be a TLR7 stimulator en pDC.[20] Interestingly, it has been suggested that mTORC1, TBK1 and IRF7 are linked with each other in peripheral lysosomes for the induction of IFN-I, and that the recruitment of mTORC1 is regulated by cholesterol.[73] The link between the cholesterol binding properties of SIDT1 and its control of the IRF7 pathway in response to TLR7 and TLR9 stimulation is under investigation.

It has been recently reported that SIDT2 could be mediating the exit of dsRNA from the lysosome for immune recognition by cytosolic sensors, but not

endosomal TLR.[25] SIDT2 is a broadly expressed protein, while SIDT1 is more restricted to lymphoid leukocytes, indicating that SIDT1 could have a more specialized immune function. A recent article provided indirect evidence about a possible role of SIDT1 in the cytosolic escape of dsRNA to the cytosol,[26] however our data do not support this hypothesis. From our results, the role of SIDT1 in the control of the access of TLR ligands to the acidic vesicles specialized in the IFN signaling[15] can easily explain the specificity of the effect in TBK1/IRF7 axis.

Inappropriate recognition of host-derived nucleic acids associated with high IFN-I production by pDC can lead to autoimmune or autoinflammatory responses.[74] Interestingly, when SIDT1-coexpressed genes were searched in skin-related data sets using SEEK, samples from psoriasis patients were top-ranking (table S1, skin dataset sheet) and SIDT1 was found to be overexpressed in the lesional skin of psoriasis patients (Figure S6), supporting the translation of the mouse results to the human disease. Using the acute model of imiquimod-induced (Aldara) psoriasiform dermatitis we have demonstrated the role of SIDT1 in the induction of pathological IFN-I responses. Firstly, *sidt1*$^{-/-}$ splenocytes and BM-pDC cultures secreted specifically less IFN-I after stimulation with exogenous nucleic acids accompanied by a lower IRF7 nuclear translocation. Secondly, the maturation and production of the pro-inflammatory cytokine TNFα and the translocation of NF-κB were not affected. Finally, *sidt1*$^{-/-}$ animals showed lower level of IFN-I in serum after Aladara treatment, and significantly reduced severity scores in the treated area at both the macroscopic and microscopic levels. All these signs of lower severity were associated with a reduction in splenomegaly and lower concentration of IFN-dependent chemokines in the skin, previously described as severity biomarkers in human and mouse psoriasis.[55,56] Similar protection levels have been reported using knock-out animals for the IL23/IL17 pathway[33] or by using immunemodulatory drugs.[54] In summary, our findings have led to the identification of SIDT1 as a new player in the induction of IFN-I responses after endosomal TLR7 and TLR9 stimulation by exogenous nucleic acids. This finding opens the way to the design of agents that modulate SIDT1 function to ameliorate the life of psoriasis patients. The highly restricted expression pattern of SIDT1 can be a valuable feature in the search for drug targets with low potential side effects. Complementary experiments are also needed to understand the role of SIDT1 in other autoimmune diseases mediated by IFN type I responses.

Declaration of interests

The authors declare that no conflict of interest exists.

Contributors

María Morell: Conceptualization, Methodology, Validation, Formal analysis, Investigation, Writing, Visualization and Supervision; **Nieves Varela:** Validation, Formal analysis, and Investigation; **Casimiro Castillejo-López** and **Céline Coppard**: Resources and investigation; **Natividad Martín and Francisco O'Valle**: Investigation, Formal analysis; **Francisco Pérez-Cózar, Gonzalo Gómez-Hernández, María José Luque** and **Ying-Yu Wu:** Validation, Formal analysis, and Investigation; **Ramesh Kumar**: Methodology; **Marta E. Alarcón-Riquelme**: Funding acquisition, resources, methodology; **Concepción Marañón**: Conceptualization, supervision, writing, funding acquisition. All authors read and approved the final version of this manuscript.

Acknowledgments

We acknowledge Pedro Carmona and Luis Javier Martínez for their valuable help in the microarray experiments, and Raquel Marrero and Sara Moreno for their help with microscopy. We also acknowledge the anonymous healthy donors for their generous blood donation. Funding was obtained from the Consejería de Salud de la Junta de Andalucía (PIER-0118-2019 and C2_S0050) and Instituto de Salud Carlos III (PI18/00082 and PI21/01151), partly supported by European FEDER funds, and prior funding to MEAR from the Alliance for Lupus Research and the Swedish Research Council.

Data sharing statement

Gene expression data have been deposited in NCBI-GEO (http://www.ncbi.nlm.nih.gov/geo/) and are accessible through accession number GSE124941.

Supplementary materials

Supplementary material associated with this article can be found, in the online version, at doi:10.1016/j.ebiom.2021.103808.

References

1 Yao Y, Richman L, Morehouse C, et al. Type I interferon: potential therapeutic target for psoriasis? *PLoS One*. 2008;3:e2737. https://doi.org/10.1371/journal.pone.0002737.
2 Lowes MA, Suarez-Farinas M, Krueger JG. Immunology of psoriasis. *Annu Rev Immunol*. 2014;32:227–255. https://doi.org/10.1146/annurev-immunol-032713-120225.
3 Nestle FO, Conrad C, Tun-Kyi A, et al. Plasmacytoid predendritic cells initiate psoriasis through interferon-alpha production. *J Exp Med*. 2005;202:135–143. https://doi.org/10.1084/jem.20050500.
4 Mylonas A, Conrad C. Psoriasis: classical vs. paradoxical. The Yin-Yang of TNF and type I interferon. *Front Immunol*. 2018;9:2746. https://doi.org/10.3389/fimmu.2018.02746.
5 Chasset F, Dayer JM, Chizzolini C. Type I interferons in systemic autoimmune diseases: distinguishing between afferent and efferent functions for precision medicine and individualized treatment. *Front Pharmacol*. 2021;12: 633821. https://doi.org/10.3389/fphar.2021.633821. 2021/05/15.
6 Liu YJ. IPC: professional type 1 interferon-producing cells and plasmacytoid dendritic cell precursors. *Annu Rev Immunol*. 2005;23:275–306. https://doi.org/10.1146/annurev.immunol.23.021704.115633.

7 Eloranta ML, Gunnar A, Ronnblom L. Plasmacytoid dendritic cells and their role in autoimmune rheumatic diseases. *Arthritis Rheum*. 2012. https://doi.org/10.1002/art.37821. 2013/01/03.
8 Saitoh S, Miyake K. Regulatory molecules required for nucleotide-sensing Toll-like receptors. *Immunol Rev*. 2009;227:32–43. 2009/01/06IMR729 [pii]10.1111/j.1600-065X.2008.00729.x.
9 Saadeh D, Kurban M, Abbas O. Update on the role of plasmacytoid dendritic cells in inflammatory/autoimmune skin diseases. *Exp Dermatol*. 2016;25:415–421. https://doi.org/10.1111/exd.12957.
10 Sozzani S, Del Prete A, Bosisio D. Dendritic cell recruitment and activation in autoimmunity. *J Autoimmun*. 2017;85:126–140. https://doi.org/10.1016/j.jaut.2017.07.012.
11 Poux C, Dondalska A, Bergenstrahle J, et al. A single-stranded oligonucleotide inhibits toll-like receptor 3 activation and reduces influenza A (H1N1) infection. *Front Immunol*. 2019;10:2161. https://doi.org/10.3389/fimmu.2019.02161.
12 Hadjadj J, Yatim N, Barnabei L, et al. Impaired type I interferon activity and inflammatory responses in severe COVID-19 patients. *Science*. 2020;369:718–724. https://doi.org/10.1126/science.abc6027.
13 Latz E, Schoenemeyer A, Visintin A, et al. TLR9 signals after translocating from the ER to CpG DNA in the lysosome. *Nat Immunol*. 2004;5:190–198. https://doi.org/10.1038/ni1028.
14 Tatematsu M, Funami K, Ishii N, et al. LRRC59 regulates trafficking of nucleic acid-sensing TLRs from the endoplasmic reticulum via association with UNC93B1. *J Immunol*. 2015;195:4933–4942. https://doi.org/10.4049/jimmunol.1501305.
15 Sasai M, Linehan MM, Iwasaki A. Bifurcation of Toll-like receptor 9 signaling by adaptor protein 3. *Science*. 2010;329:1530–1534. https://doi.org/10.1126/science.1187029.
16 BL L, Barton GM. Trafficking of endosomal Toll-like receptors. *Trends Cell Biol*. 2014;24:360–369. https://doi.org/10.1016/j.tcb.2013.12.002.
17 Guo H, Zhang J, Zhang X, et al. SCARB2/LIMP-2 regulates IFN production of plasmacytoid dendritic cells by mediating endosomal translocation of TLR9 and nuclear translocation of IRF7. *J Immunol*. 2015;194:4737–4749. https://doi.org/10.4049/jimmunol.1402312.
18 Schwartz JA, Clayton KL, Mujib S, et al. Tim-3 is a marker of plasmacytoid dendritic cell dysfunction during HIV infection and is associated with the recruitment of IRF7 and p85 into lysosomes and with the submembrane displacement of TLR9. *J Immunol*. 2017;198:3181–3194. https://doi.org/10.4049/jimmunol.1601298.
19 Gardet A, Pellerin A, McCarl CA, et al. Effect of *in vivo* hydroxychloroquine and *ex vivo* anti-BDCA2 mAb treatment on pDC IFNalpha production from patients affected with cutaneous Lupus Erythematosus. *Front Immunol*. 2019;10:275. https://doi.org/10.3389/fimmu.2019.00275.
20 Salvi V, Gianello V, Busatto S, et al. Exosome-delivered microRNAs promote IFN-alpha secretion by human plasmacytoid DCs via TLR7. *JCI Insight*. 2018;3. https://doi.org/10.1172/jci.insight.98204.
21 Murayama G, Furusawa N, Chiba A, et al. Enhanced IFN-alpha production is associated with increased TLR7 retention in the lysosomes of palasmacytoid dendritic cells in systemic lupus erythematosus. *Arthritis Res Ther*. 2017;19:234. https://doi.org/10.1186/s13075-017-1441-7.
22 Valdes VJ, Athie A, Salinas LS, et al. CUP-1 is a novel protein involved in dietary cholesterol uptake in Caenorhabditis elegans. *PLoS One*. 2012;7:e33962. https://doi.org/10.1371/journal.pone.0033962.
23 Mendez-Acevedo KM, Valdes VJ, Asanov A, et al. A novel family of mammalian transmembrane proteins involved in cholesterol transport. *Sci Rep*. 2017;7:7450. https://doi.org/10.1038/s41598-017-07077-z.
24 Otarigho B, Aballay A. Cholesterol regulates innate immunity via nuclear hormone receptor NHR-8. *iScience*. 2020;23: 101068. https://doi.org/10.1016/j.isci.2020.101068.
25 Nguyen TA, Smith BRC, Tate MD, et al. SIDT2 transports extracellular dsRNA into the cytoplasm for innate immune recognition. *Immunity*. 2017;47:498–509. https://doi.org/10.1016/j.immuni.2017.08.007. e496.
26 Nguyen TA, Smith BRC, Elgass KD, et al. SIDT1 localizes to endolysosomes and mediates double-stranded RNA transport into the cytoplasm. *J Immunol*. 2019. https://doi.org/10.4049/jimmunol.1801369.
27 Grine L, Dejager L, Libert C, et al. Dual inhibition of TNFR1 and IFNAR1 in imiquimod-induced psoriasiform skin inflammation in mice. *J Immunol*. 2015;194:5094–5102. https://doi.org/10.4049/jimmunol.1403015.
28 Austin CP, Battey JF, Bradley A, et al. The knockout mouse project. *Nat Genet*. 2004;36:921–924. https://doi.org/10.1038/ng0904-921.
29 Chen Q, Zhang F, Dong L, et al. SIDT1-dependent absorption in the stomach mediates host uptake of dietary and orally administered microRNAs. *Cell Res*. 2020. https://doi.org/10.1038/s41422-020-0389-3.
30 Chaperot L, Blum A, Manches O, et al. Virus or TLR agonists induce TRAIL-mediated cytotoxic activity of plasmacytoid dendritic cells. *J Immunol*. 2006;176:248–255. 2005/12/21. 176/1/248 [pii].
31 Kato H, Sato S, Yoneyama M, et al. Cell type-specific involvement of RIG-I in antiviral response. *Immunity*. 2005;23:19–28. https://doi.org/10.1016/j.immuni.2005.04.010.
32 Vremec D. The isolation and enrichment of large numbers of highly purified mouse spleen dendritic cell populations and their *in vitro* equivalents. *Methods Mol Biol*. 2016;1423:61–87. https://doi.org/10.1007/978-1-4939-3606-9_5.
33 van der Fits L, Mourits S, Voerman JS, et al. Imiquimod-induced psoriasis-like skin inflammation in mice is mediated via the IL-23/IL-17 axis. *J Immunol*. 2009;182:5836–5845. https://doi.org/10.4049/jimmunol.0802999.
34 Ueyama A, Yamamoto M, Tsujii K, et al. Mechanism of pathogenesis of imiquimod-induced skin inflammation in the mouse: a role for interferon-alpha in dendritic cell activation by imiquimod. *J Dermatol*. 2014;41:135–143. https://doi.org/10.1111/1346-8138.12367.
35 Suvarna KS, Layton C, Bancroft JD. *Bancroft's Theory and Practice of Histological Techniques*. 8 ed. Elsevier; 2019:584.
36 Carmona-Saez P, Chagoyen M, Tirado F, et al. GENECODIS: a web-based tool for finding significant concurrent annotations in gene lists. *Genome Biol*. 2007;8:R3 https://doi.org/10.1186/gb-2007-8-1-r3. 2007/01/06. gb-2007-8-1-r3 [pii].
37 Herwig R, Hardt C, Lienhard M, et al. Analyzing and interpreting genome data at the network level with ConsensusPathDB. *Nat Protoc*. 2016;11:1889–1907. https://doi.org/10.1038/nprot.2016.117.
38 Zhu Q, Wong AK, Krishnan A, et al. Targeted exploration and analysis of large cross-platform human transcriptomic compendia. *Nat Methods*. 2015;12:211–214. https://doi.org/10.1038/nmeth.3249.
39 Delgado-Vega AM, Dozmorov MG, Quiros MB, et al. Fine mapping and conditional analysis identify a new mutation in the autoimmunity susceptibility gene BLK that leads to reduced half-life of the BLK protein. *Ann Rheum Dis*. 2012;71:1219–1226. https://doi.org/10.1136/annrheumdis-2011-200987. 2012/06/15annrheumdis-2011-200987 [pii].
40 Manders EMM, Verbeek FJ, Aten JA. Measurement of co-localization of objects in dual-colour confocal images. *J Microsc*. 1993;169:375–382. https://doi.org/10.1111/j.1365-2818.1993.tb03313.x.
41 Lenth RV. Statistical power calculations. *J Anim Sci*. 2007;85:E24–E29. https://doi.org/10.2527/jas.2006-449.
42 Wu C, Jin X, Tsueng G, et al. BioGPS: building your own mash-up of gene annotations and expression profiles. *Nucleic Acids Res*. 2016;44:D313–D316. https://doi.org/10.1093/nar/gkv1104.
43 Su AI, Wiltshire T, Batalov S, et al. A gene atlas of the mouse and human protein-encoding transcriptomes. *Proc Natl Acad Sci U S A*. 2004;101:6062–6067. https://doi.org/10.1073/pnas.0400782101.
44 Carmona-Saez P, Varela N, Luque MJ, et al. Metagene projection characterizes GEN2.2 and CAL-1 as relevant human plasmacytoid dendritic cell models. *Bioinformatics*. 2017;33:3691–3695. https://doi.org/10.1093/bioinformatics/btx502.
45 Kadowaki N, Ho S, Antonenko S, et al. Subsets of human dendritic cell precursors express different toll-like receptors and respond to different microbial antigens. *J Exp Med*. 2001;194:863–869. https://doi.org/10.1084/jem.194.6.863.
46 Winston WM, Molodowitch C, Hunter CP. Systemic RNAi in C. elegans requires the putative transmembrane protein SID-1. *Science*. 2002;295:2456–2459. https://doi.org/10.1126/science.1068836.
47 Li W, Koutmou KS, Leahy DJ, et al. Systemic RNA interference deficiency-1 (SID-1) extracellular domain selectively binds long double-stranded RNA and is required for RNA transport by SID-1. *J Biol Chem*. 2015;290:18904–18913. https://doi.org/10.1074/jbc.M115.658864.
48 Tenoever BR, Ng SL, Chua MA, et al. Multiple functions of the IKK-related kinase IKKepsilon in interferon-mediated antiviral immunity. *Science*. 2007;315:1274–1278. https://doi.org/10.1126/science.1136567.
49 Bodewes ILA, Huijser E, van Helden-Meeuwsen CG, et al. TBK1: A key regulator and potential treatment target for interferon positive Sjogren's syndrome, systemic lupus erythematosus and systemic sclerosis. *J Autoimmun*. 2018;91:97–102. https://doi.org/10.1016/j.jaut.2018.02.001.

50 Honda K, Ohba Y, Yanai H, et al. Spatiotemporal regulation of MyD88-IRF-7 signalling for robust type-I interferon induction. *Nature*. 2005;434:1035–1040. https://doi.org/10.1038/nature03547.

51 Marie I, Smith E, Prakash A, et al. Phosphorylation-induced dimerization of interferon regulatory factor 7 unmasks DNA binding and a bipartite transactivation domain. *Mol Cell Biol*. 2000;20:8803–8814. https://doi.org/10.1128/MCB.20.23.8803-8814.2000.

52 Stockenhuber K, Hegazy AN, West NR, et al. Foxp3(+) T reg cells control psoriasiform inflammation by restraining an IFN-I-driven CD8(+) T cell response. *J Exp Med*. 2018;215:1987–1998. https://doi.org/10.1084/jem.20172094.

53 Zapi-Colin LA, Gutierrez-Gonzalez G, Rodriguez-Martinez S, et al. A peptide derived from phage-display limits psoriasis-like lesions in mice. *Heliyon*. 2020;6:e04162. https://doi.org/10.1016/j.heliyon.2020.e04162.

54 Lin ZM, Ma M, Li H, et al. Topical administration of reversible SAHH inhibitor ameliorates imiquimod-induced psoriasis-like skin lesions in mice via suppression of TNF-alpha/IFN-gamma-induced inflammatory response in keratinocytes and T cell-derived IL-17. *Pharmacol Res*. 2018;129:443–452. https://doi.org/10.1016/j.phrs.2017.11.012.

55 McColl A, Thomson CA, Nerurkar L, et al. TLR7-mediated skin inflammation remotely triggers chemokine expression and leukocyte accumulation in the brain. *J Neuroinflammation*. 2016;13:102. https://doi.org/10.1186/s12974-016-0562-2.

56 Fitzgerald O, Chandran V. Update on biomarkers in psoriatic arthritis: a report from the GRAPPA 2010 annual meeting. *J Rheumatol*. 2012;39:427–430. https://doi.org/10.3899/jrheum.111241.

57 Baccala R, Hoebe K, Kono DH, et al. TLR-dependent and TLR-independent pathways of type I interferon induction in systemic autoimmunity. *Nat Med*. 2007;13:543–551. https://doi.org/10.1038/nm1590.

58 Sa Ribero M, Jouvenet N, Dreux M, et al. Interplay between SARS-CoV-2 and the type I interferon response. *PLoS Pathog*. 2020;16:e1008737. https://doi.org/10.1371/journal.ppat.1008737.

59 Azar P, Mejia JE, Cenac C, et al. TLR7 dosage polymorphism shapes interferogenesis and HIV-1 acute viremia in women. *JCI Insight*. 2020;5(12):e136047. https://doi.org/10.1172/jci.insight.136047.

60 Kawai T, Akira S. The role of pattern-recognition receptors in innate immunity: update on Toll-like receptors. *Nat Immunol*. 2010;11:373–384. https://doi.org/10.1038/ni.1863.

61 Lee BL, Moon JE, Shu JH, et al. UNC93B1 mediates differential trafficking of endosomal TLRs. *Elife*. 2013;2:e00291. https://doi.org/10.7554/eLife.00291.

62 Leifer CA, Brooks JC, Hoelzer K, et al. Cytoplasmic targeting motifs control localization of toll-like receptor 9. *J Biol Chem*. 2006;281:35585–35592. https://doi.org/10.1074/jbc.M607511200.

63 Hayashi K, Sasai M, Iwasaki A. Toll-like receptor 9 trafficking and signaling for type I interferons requires PIKfyve activity. *Int Immunol*. 2015;27:435–445. https://doi.org/10.1093/intimm/dxv021.

64 Martinson JA, Montoya CJ, Usuga X, et al. Chloroquine modulates HIV-1-induced plasmacytoid dendritic cell alpha interferon: implication for T-cell activation. *Antimicrob Agents Chemother*. 2010;54:871–881. https://doi.org/10.1128/AAC.01246-09.

65 Antonczyk A, Krist B, Sajek M, et al. Direct inhibition of IRF-dependent transcriptional regulatory mechanisms associated with disease. *Front Immunol*. 2019;10:1176. https://doi.org/10.3389/fimmu.2019.01176.

66 Hasan M, Yan N. Therapeutic potential of targeting TBK1 in autoimmune diseases and interferonopathies. *Pharmacol Res*. 2016;111:336–342. https://doi.org/10.1016/j.phrs.2016.04.008. 2016/06/30.

67 Hasan M, Koch J, Rakheja D, et al. Trex1 regulates lysosomal biogenesis and interferon-independent activation of antiviral genes. *Nat Immunol*. 2013;14:61–71. https://doi.org/10.1038/ni.2475.

68 Motani K, Ito S, Nagata S. DNA-mediated cyclic GMP-AMP synthase-dependent and -independent regulation of innate immune responses. *J Immunol*. 2015;194:4914–4923. https://doi.org/10.4049/jimmunol.1402705.

69 Suzuki T, Oshiumi H, Miyashita M, et al. Cell type-specific subcellular localization of phospho-TBK1 in response to cytoplasmic viral DNA. *PLoS One*. 2013;8:e83639. https://doi.org/10.1371/journal.pone.0083639.

70 Zhu X, Owen JS, Wilson MD, et al. Macrophage ABCA1 reduces MyD88-dependent toll-like receptor trafficking to lipid rafts by reduction of lipid raft cholesterol. *J Lipid Res*. 2010;51:3196–3206. https://doi.org/10.1194/jlr.M006486.

71 Monson EA, Crosse KM, Das M, et al. Lipid droplet density alters the early innate immune response to viral infection. *PLoS One*. 2018;13:e0190597. https://doi.org/10.1371/journal.pone.0190597.

72 Saitoh T, Satoh T, Yamamoto N, et al. Antiviral protein Viperin promotes toll-like receptor 7- and Toll-like receptor 9-mediated type I interferon production in plasmacytoid dendritic cells. *Immunity*. 2011;34:352–363. https://doi.org/10.1016/j.immuni.2011.03.010. 2011/03/26. S1074-7613(11)00088-4.

73 Miyake K, Saitoh SI, Sato R, et al. Endolysosomal compartments as platforms for orchestrating innate immune and metabolic sensors. *J Leukoc Biol*. 2019;106:853–862. https://doi.org/10.1002/JLB.MR0119-020R. 20190620.

74 Takagi H, Arimura K, Uto T, et al. Plasmacytoid dendritic cells orchestrate TLR7-mediated innate and adaptive immunity for the initiation of autoimmune inflammation. *Sci Rep*. 2016;6:24477. https://doi.org/10.1038/srep24477.